9-2020

Investigation of Factors Impacting a Helicopter Height-Velocity Diagram

Timothy A. Brown

INVESTIGATION OF FACTORS IMPACTING A HELICOPTER HEIGHT-VELOCITY DIAGRAM

THESIS

Timothy Aaron Brown, 1st Lt, USAF

AFIT-ENY-MS-20-S-084

DEPARTMENT OF THE AIR FORCE
AIR UNIVERSITY

AIR FORCE INSTITUTE OF TECHNOLOGY

Wright-Patterson Air Force Base, Ohio

AFIT-ENY-MS-20-S-084

INVESTIGATION OF FACTORS IMPACTING A HELICOPTER HEIGHT-VELOCITY DIAGRAM

THESIS

Presented to the Faculty

Department of Aeronautical Engineering

Graduate School of Engineering and Management

Air Force Institute of Technology

Air University

Air Education and Training Command

in Partial Fulfillment of the Requirements for the

Degree of Master of Science in Aeronautical Engineering

Timothy Aaron Brown, B.S.

1st Lt, USAF

2020

AFIT-ENY-MS-20-S-084

INVESTIGATION OF FACTORS IMPACTING A HELICOPTER HEIGHT-VELOCITY DIAGRAM

Timothy Aaron Brown, B.S.
1st Lt, USAF

Committee Membership:

Dr. Donald Kunz
Chair

Maj Joshuah Hess, PhD
Member

Dr. Richard Cobb
Member

Abstract

A dynamic helicopter model was incorporated into an optimal control problem to determine minimal landing velocities. The solutions were determined using pseudospectral collocation methods as implemented by the GPOPS-II software. These solutions were then compiled to develop a Height-Velocity (HV) diagram. An HV diagram displays regions of flight based on a helicopter's airspeed and height above the ground in which a safe landing would not be possible following engine failure. The applied methodology for constructing the HV diagram reduced issues involving solution convergence that was encountered in previous research. The influence of ground effect on the dynamic model was also investigated. After analyzing the HV diagrams constructed using five additional ground effect models, the significant impact that a chosen ground effect model has in the overall dynamic model was apparent. Finally, the effect that modifying certain helicopter parameters has on the helicopter's autorotation performance was considered. Optimal control solutions showed a decrease in autorotation capabilities for the case of an increased gross weight as well as for the case of a decreased rotor size.

Acknowledgments

First, I would like to thank my advisor, Dr. Kunz, for all that he did to help me with this research. He was extremely helpful in providing guidance and suggesting new courses of action for whenever I hit road blocks in my research. He showed extreme patience with me during a very difficult time for me. I am very grateful to him.

I would also like to thank Dr. Cobb and Major Hess. Their instruction over the course of several classes helped me gain a better understanding of control theory and optimization that was instrumental to this research. In addition, they provided excellent constructive feedback on my thesis.

Finally, I would like to thank my family and close friends for their constant support.

Soli Deo Gloria.

Timothy Aaron Brown

Table of Contents

Page

List of Figures

List of Tables

List of Acronyms

AI Autorotation Index

FAA Federal Aviation Administration

HDP Helicopter Dynamic Performance

HV Height-Velocity

KKT Karush-Kuhn-Tucker

LG Legendre-Gauss

LGL Legendre-Gauss-Lobatto

LGR Legendre-Gauss-Radau

MATLAB Matrix Laboratory

NAVAIR Naval Air Systems Command

NLP nonlinear programming

OEI one engine inoperable

SGR Sequential Gradient Restoration

SQP Sequential Quadratic Programming

VRS vortex ring state

VTOL Vertical Takeoff and Landing

List of Symbols

α	Rotor Tip Path Plane Angle with Horizon
η_C	Combined Gearbox Efficiency
η_{MR}	Main Rotor Gearbox Efficiency
η_{TR}	Tail Rotor Gearbox Efficiency
λ	Inflow Ratio
μ	Advance Ratio
μ_x	Rotor Radial Velocity Ratio
μ_z	Rotor Axial Velocity Ratio
Ω	Rotor Angular Velocity
Ω_{TR}	Tail Rotor Angular Velocity
σ	Solidity
τ_1	Engine 1 Time Constant
τ_2	Engine 2 Time Constant
θ_{FP}	Flight Path Angle
A	Main Rotor Disk Plane Area
A_{TR}	Tail Rotor Disk Plane Area
AI	Autorotation Index
C_T	Thrust Coefficient
c_{do}	Blade Drag Coefficient
$C_{T_{TR}}$	Tail Rotor Thrust Coefficient
C_{Tx}	Horizontal Component of Thrust Coefficient
C_{Tz}	Vertical Component of Thrust Coefficient
D	Drag
DL	Disk Loading
f	Equivalent Planform Flat Plate Area
g	Gravitational Acceleration
h	Altitude Above Ground Level
I_R	Rotor Polar Moment of Inertia
k_g	Ground Effect Factor
k_i	Induced Power Correction Factor
l_{TR}	Distance Between Main Rotor and Tail Rotor
m	Aircraft Mass
M_{TR}	Tail Rotor Moment
P_R	Required Power
P_S	Power Supplied by Engine
P_{Acc}	Accessory Power Loss
P_{MR}	Main Rotor Required Power
P_{TR}	Tail Rotor Required Power
Q_{Req}	Torque Required
R_{TR}	Tail Rotor Radius
T	Thrust
T_{TR}	Tail Rotor Thrust
u	Horizontal Velocity
V	Aircraft Velocity
w	Vertical Velocity
x	Horizontal Position

INVESTIGATION OF FACTORS IMPACTING A HELICOPTER HEIGHT-VELOCITY DIAGRAM

I. Introduction

1.1 Chapter Overview

When a helicopter loses engine power, the pilot must perform a maneuver called autorotation to land the aircraft. The ability for a helicopter to land safely depends on a number of factors including helicopter properties, altitude, and airspeed. The compilation of these factors in a Height-Velocity (HV) diagram informs pilots on which regions of flight are hazardous in case of engine failure and would not allow for a safe landing. Continuing the work completed by Harris [2], this research focuses on analyzing autorotation characteristics and developing a method to analytically derive a helicopter's HV diagram using optimal control theory. This chapter introduces the concepts of autorotation and HV diagrams and then provides the scope and objectives of this research.

1.2 Autorotation

The term autorotation refers to the state of flight where a helicopter descends while one or more of its engine is no longer providing power to the main rotor. Without engine power, the rotor continues to spin due to power provided to it by the upward airflow through the rotor. This rotorcraft flight condition is analogous to the glide of a fixed-wing aircraft; lift is still produced but at a much lesser extent than during normal operations with full engine power. Autorotations are typically performed

during emergencies after a helicopter experiences a mechanical failure of either the engine, driveshaft, or tail rotor. Autorotations oftentimes provide the fastest rate of descent for a helicopter to land. Consequently, an autorotation is also commonly performed when there are other emergencies on board, such as a fire or control system malfunction, requiring the helicopter to land quickly [5].

An autorotation maneuver can be described in three basic phases, which are discussed in more detail in rotorcraft flight handbooks such as [5] and [6]. The first phase is the entry into autorotation, which occurs immediately after the helicopter loses engine power. Initially, the rotor slows down, since it no longer has the power required to maintain its previous flight condition. The collective pitch should then be lowered to decrease the rotor's drag and lift. This sends the helicopter into a dive. The air flowing upward through the descending rotor then provides enough energy to support a functional rotor angular velocity. The pilot's reaction time during this initial phase significantly affects the autorotation. The next phase is steady-state autorotation during which the helicopter continues to descend to maintain its rotor speed. As the helicopter approaches the ground, it dissipates its forward and vertical velocities by performing a flare before landing. A flare describes a maneuver in which the aircraft's nose is raised in order to decrease the velocity of the aircraft before landing. During the flare, the airflow through the rotor increases, thereby generating more lift and slowing the helicopter. The rotor speed also decreases during the flare. Finally, the pilot levels the helicopter in order to land without hitting the ground with the tail. Figure 1.1 illustrates these phases of an autorotation.

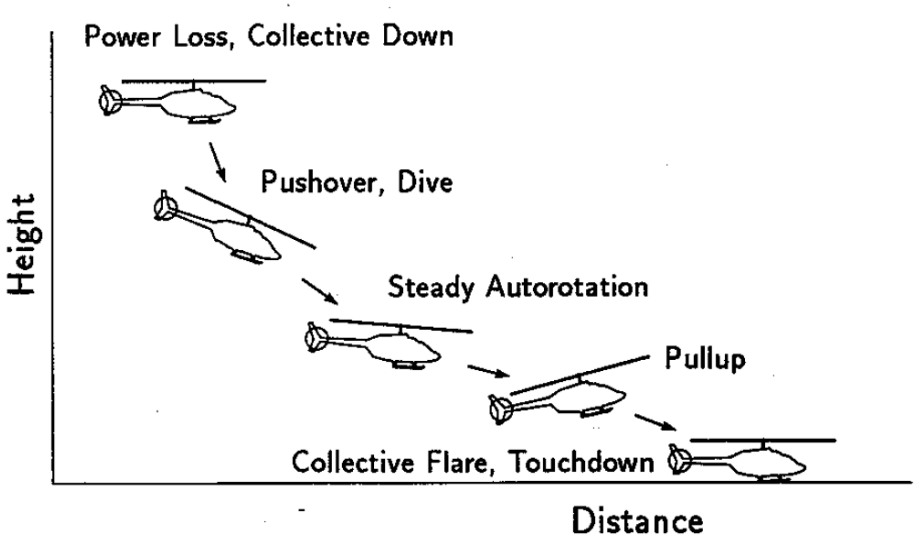

Figure 1.1. A Helicopter During Autorotation [1]

1.3 HV Diagram

The ability for a helicopter to land safely within its structural limits following an autorotation is contingent on the helicopter's initial forward airspeed and height above the ground when engine power is lost. HV diagrams show the combination of these two factors based on the particular helicopter in question, the gross weight, and density altitude. Figure 1.2 shows an example HV diagram for low-speed flight. The shaded portion of the diagram depicts the unsafe flight region in which a safe landing could not occur if engine failure occurs. In this region, the rotor speed does not have enough time to recover after its initial drop to perform a successful flare. Without a successful flare, the helicopter impacts the ground at a damaging velocity. The dividing curve between the safe and unsafe regions on the HV diagram is referred to as the "deadman's curve" and includes three key, defining points: the low hover point, high hover point, and knee point. The two hover points represent the lowest and highest points on the curve, respectively. Above the upper portion of the curve, the rotor speed can recover enough during the descent to flare and thus land safely. Below the lower portion of the curve, the height of the helicopter above the ground is

not high enough for the helicopter to accelerate to unrecoverable speeds, since it will touch down on the ground very quickly after the power loss. Hence, the power loss in this region allows for a safe landing. As forward airspeed increases, the autorotative descent rate decreases [7]. This leads to the knee point where the upper and lower portions of the curve intersect. HV diagrams typically also have a high-speed unsafe region near the ground where the helicopter's high airspeed does not allow for a sufficient reduction in velocity before hitting the ground. These two unsafe regions help create a flight path for pilots to follow during routine takeoffs and landings by displaying flight regions to avoid.. This research focused on the low-speed portion of the HV diagram.

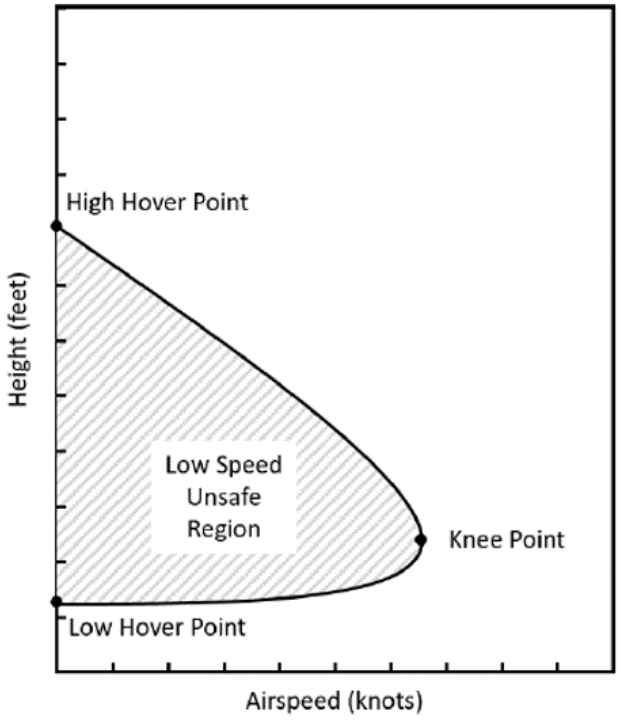

Figure 1.2. Example Height-Velocity Diagram [2]

As described above, HV diagrams inform pilots of which regions of flight would be hazardous if engine failure were to occur there. In addition to having HV diagrams for total engine power loss, multi-engine rotorcraft have separate HV diagrams for one

engine inoperable (OEI) flight in which only one engine fails. Naturally, the unsafe region is smaller for OEI flight than for total power loss, since there is still some power supplied to the rotor from the remaining engine(s). With multiple engines, the chances of total power loss is significantly reduced. Since many military helicopters have two engines, there is a need for accurate OEI HV diagrams in addition to the total power loss diagrams.

Due to the implicit risks and expenses involved in conducting flight tests that involve determining the limitations of safe flight, HV diagrams are usually produced using analytical methods. Based on the analytical solutions, flight tests are performed at select locations on the diagram to validate the results. This greatly reduces the number of flight tests needed to determine the HV envelopes for a given helicopter at various altitude densities and gross weights. (See Reference [8] for a summary of an extensive test campaign to construct the HV diagrams for an AH-1G helicopter at two additional gross weights that had not been previously tested.) It is thus essential to have accurate analytical methods to estimate the deadman's curve. Optimal control theory has been utilized during past research as an effective tool in providing these analytical means. By analyzing the optimal flight trajectories for several test cases, the limitations of safe flight as described by an HV diagram can be estimated..

1.4 Research Catalyst

The Naval Air Systems Command (NAVAIR) is responsible for the acquisition, testing, and management of aircraft for the Navy and Marine Corps. NAVAIR has a need for additional methods for validating the HV data supplied to them by rotorcraft manufacturers. This research will supplement the analytical methods available to NAVAIR in calculating HV curves for rotorcraft in OEI flight. Additionally, this research will provide an archetype for investigating autorotative characteristics using

optimal control methods.

1.5 Research Objectives

This research aims to contribute to the increased understanding of autorotation capabilities, specifically with regards to limits on the safe helicopter flight envelope. The objectives of this research are as follows:

- Develop an improved mathematical model for helicopter dynamics.
- Analyze the trajectory of a helicopter during autorotation using optimal control.
- Implement a more robust optimal control solution process to derive a more defined HV diagram.
- Determine the influence of ground effect in the dynamic model.
- Examine the effects of changes in helicopter properties on a helicopter's autorotative capabilities.

1.6 Thesis Overview

This chapter has introduced the topic of helicopter HV diagrams as well as provided the main objectives of this research. Chapter 2 provides background on prior research into the construction of HV diagrams, an overview of optimal control theory, and the application of optimal control to the autorotation problem. Chapter 3 discusses the methodology used in this research to develop a dynamic model of helicopter flight, formulate an optimal control problem to use in constructing a HV diagram, and investigate autorotative characteristics. Chapter 4 provides the results of the autorotation investigation as well as the solutions to the optimal control problem. Chapter 5 discusses conclusions from this research and recommendations for further research.

II. Background

2.1 Chapter Overview

This chapter discusses previous research into the construction of Height-Velocity (HV) diagrams, which has transitioned from initially being solely empirically based to now incorporating analytical methods to supplement flight tests. The majority of current analytical methods for estimating HV curves apply optimal control theory to analyze autorotation trajectories. This chapter provides an overview of optimal control, focusing on the methods used in this research. The development of rotorcraft dynamic models along with the application of optimal control to those models is then discussed. Finally, a brief background of autorotation indices which have previously been applied to analyze autorotation performance is presented.

2.2 Early Height Velocity Research

2.2.1 HV Flight Tests

Initial investigations into the safe regions of helicopter flight described by HV diagrams involved empirical analysis of helicopters during autorotation following power failure. While autorotation was already a commonly taught maneuver by the onset of the 1950's, very little was known at that time about what heights were sufficient to allow for successful autorotation and a safe landing. The first attempts to determine these required heights were flight tests during which the helicopter's engine would be shut off to simulate engine failure. O'Hara and Mather [9] reported the findings of one such series of flight tests conducted by the Aeronautical Research Council in 1951. These tests measured the amount of height lost for the test helicopter, the *Hoverfly I*, during autorotations at various initial heights and forward velocities. Based on these measurements, the general trend of an unsafe flight envelope with an upper

bound that decreases as forward velocity increases and a lower bound that increases as velocity increases was inferred.

In the 1960s, the Aircraft Development Service of the Federal Aviation Administration (FAA) launched a flight test program with the intent of developing a practical approach for determining the flight envelope shown in HV diagrams. This study specifically examined the effects that flight altitude and helicopter gross weight had on the low-speed HV diagrams for three different single-engine, single-rotor helicopters that varied in disk loading and rotor inertia. During each test, a simulated engine failure was executed at either a designated forward velocity with progressively lower altitudes or a designated altitude with progressively lower velocities. Based on the results of these flight tests, Hanley and Devore [10] noted that the HV diagrams for each helicopter constituted a family of curves that varied as functions of the density altitude and gross weight. After nondimensionalizing these curves using the critical velocity and critical height determined from the knee point of the HV diagram, all of the nondimensional test point values fell on the same curve. Hanley and Devore determined that HV diagrams for a given helicopter can therefore be generalized in nondimensional terms once the knee point of the flight condition in question has been determined.

2.2.2 HV Semi-Empirical Methods

Pegg [11] continued off of the work of Hanley and Devore and utilized the FAA's flight test results to develop a semi-empirical method for determining a helicopter's HV diagram. Pegg's semi-empiricial method first estimated the low hover height, high hover height, and knee point of the HV diagram, and then used those points to scale the HV curve for a given helicopter based on the flight density altitude and gross weight. For the estimation of the knee point, this method calculated the critical

velocity for each case but assumed, based on the flight data from the three test helicopters, that the critical height would remain at approximately 95 feet. Pegg's semi-empirical method served as a useful baseline for developing HV diagrams. In 1980, the Helicopter Dynamic Performance (HDP) program used Pegg's model as the basis for its construction of the HV curve [12]. As digital computing power started to provide more analytical capabilities, these early empirical and semi-empirical methods for determining HV diagrams were supplemented by more effective analytical solution methods, most notably optimal control.

2.3 Optimal Control

2.3.1 Optimal Control Overview

Optimal control theory provides a means of determining the control inputs into a system that optimize a desired performance criterion while satisfying physical constraints on the system [13]. One of the first steps in formulating an optimal control problem is to develop a mathematical model of the system being analyzed. These models are commonly represented in state variable form, consisting of a set of state variables (states), which describe specific components of the system, and control variables (controls), which describe the inputs to the system that drive the states to optimize a performance index. The state and control variables are related by a set of first-order differential equations that describe the dynamics of the system. Algebraic equations are used to describe any path constraints that may exist on each of the states and controls as well as the initial and terminal boundary conditions for the variables. Finally, a scalar performance index (or objective/cost function) is selected to be either minimized or maximized. In dynamic optimization problems, the performance index is a functional, meaning that it is a function of functions, since the state trajectory and control time history are functions [13]. The set of controls along

with the associated states that minimize the performance index while satisfying the constraints on the system constitute the solution of the optimal control problem.

In order to determine whether a solution is the minimum and thus the optimal solution, certain necessary conditions must be met. The interested reader can refer to Kirk [13] or Betts [14] for a detailed description of these necessary conditions based on the boundary conditions of the problem.

Given the complex nature of most optimal control problems, optimal control solutions are typically determined using numerical methods. Betts [15] [14] and Rao [16] provide surveys of the common numerical methods for optimal control. The two main classifications for these optimal control numerical methods are indirect methods and direct methods. Figure 2.1 shows an overview of the optimal control problem with respect to each of these methods. While explaining the fundamental differences between indirect and direct methods, Rao [16] describes the numerical methods used in optimal control as having three main components: 1) methods for solving systems of nonlinear algebraic equations, 2) methods for solving differential equations and integration functions, and 3) methods for solving nonlinear optimization problems. Indirect methods involve the first two components, 1) and 2), while direct methods involve the last two components, 2) and 3).

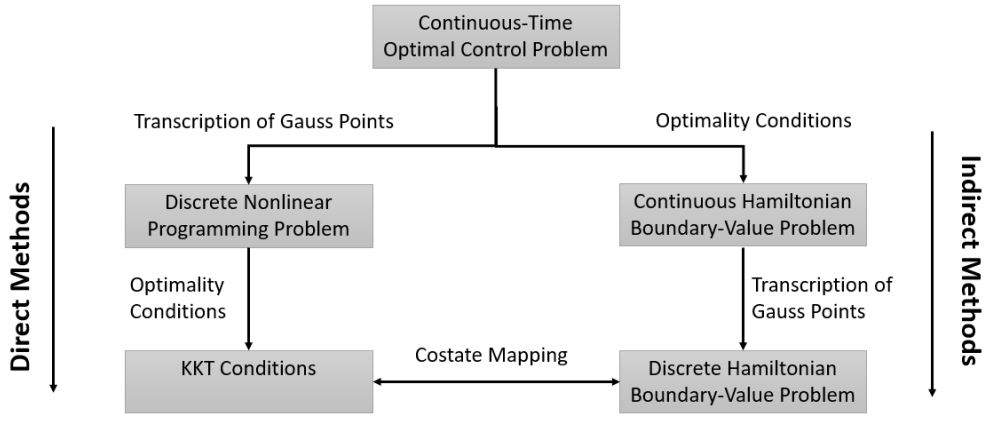

Figure 2.1. Indirect vs. Direct Methods [3]

2.3.2 Indirect Methods

Indirect methods apply the calculus of variations to the optimal control problem in order to derive the first-order necessary conditions for optimality. The necessary conditions are typically represented in terms of the Hamiltonian. The Hamiltonian is the integrand in the cost functional augmented with the system constraints and Lagrange multipliers. These Lagrange multipliers are called the costates of the system. The costates may or may not have any physical significance, depending on the system and problem formulation. The state equations are determined by taking the partial derivatives of the Hamiltonian with respect to the costates. Similarly, the costate equations are found by taking the partial derivative of the Hamiltonian with respect to the states. The partial derivative of the Hamiltonian with respect to the controls yields the control equations [13]. The Euler-Lagrange necessary conditions include this set of equations along with the boundary conditions derived from known initial states and the terminal costates. The boundary conditions (or transversality conditions) can vary based on whether the initial and terminal times/states are fixed or free. Section 5.1 of [13] summarizes the different boundary conditions for optimal control problems. The most common indirect methods for solving the resulting two-point boundary-value problem are the indirect shooting method, the indirect multiple-shooting method, and indirect collocation methods [16]. Section 4.3 of [14] lists some of the difficulties that arise when trying to solve optimal control problems using indirect methods. One of the primary difficulties is having to make a relatively accurate initial guess for the costates, which can be difficult since the costates do not always correspond to physical quantities.

2.3.3 Direct Methods

Whereas indirect methods require explicit derivation of the costate equations, control equations, and transversality conditions, direct methods do not. Rather than finding the derivatives of the Hamiltonian, direct methods discretize the continuous optimal control problem into a nonlinear programming (NLP) problem and find the resulting NLP solution. Similarly to indirect methods, the system equality and inequality constraints are appended to the cost function with Lagrange multipliers. The augmented performance index is sometimes referred to as the Lagrangian. The resulting necessary conditions for optimality are the Karush-Kuhn-Tucker (KKT) conditions. The KKT conditions are: 1) the gradient of the Lagrangian with respect to each of the states, controls, and Lagrange multipliers are zero; 2) the inequality constraints must be feasible; 3) the Lagrange multipliers for the inequality constraints posed as less than or equal to zero must be non-negative; and 4) the gradients of active constraints must be linearly independent [14]. Two of the most prevalent direct methods for solving the optimal control problem while only parameterizing the control are the direct shooting method and the direct multiple shooting method. Direct collocation methods parameterize both the states and controls in their solutions [16].

2.3.4 Nonlinear Programming

Many methods for solving optimal control problems employ nonlinear/parameter optimization or nonlinear programming. The NLP problem finds a set of discretized system parameters that minimize a performance index subject to algebraic constraints while meeting the KKT necessary conditions for optimality. The values for the parameters and their derivatives are calculated at each discretized point [15]. A NLP problem can either be classified as either dense, meaning that a large percentage of the derivatives of the cost function and constraint functions are nonzero, or sparse,

meaning that a large percentage of the derivatives of the cost function and constraint functions are zero [16]. Betts [14] details different techniques that are particularly suited for solving different NLP problems based on this classification. One of the most common methods for solving NLP problems is the Sequential Quadratic Programming (SQP) algorithm. The SQP algorithm is described in detail in several optimization textbooks, such as in Section 13.4 of [17]. Gill, Murray, and Saunders [18] developed a sparse NLP solver SNOPT, which utilizes the SQP algorithm. SNOPT is especially suitable for solving trajectory optimization problems.

2.3.5 Collocation Methods

In direct collocation methods, the problem's interval of interest is divided into mesh intervals in which the states and controls are collocated at selected points, called collocation points or nodes. The transcribed NLP problem is then solved for the states and controls at each collocation point simultaneously [19]. There are several methods of choosing the location of the collocation points. Orthogonal collocation methods select the roots of orthogonal polynomials, such as Chebyshev or Legendre polynomials, as the nodes. These methods are often favored due to their increased accuracy in quadrature approximations to definite integrals [16]. Collocation methods can also be classified as either local collocation and global collocation.

2.3.6 Pseudospectral Methods

One type of direct, global orthogonal collocation are pseudospectral methods. In pseudospectral methods, the optimal control problem is transcribed into a NLP problem using global polynomials to parameterize the states and controls, and a Gaussian quadrature to collocate the differential-algebraic equations [20]. Pseudospectral methods define the domain of the problem as [-1,1] by performing an affine transformation.

The most common sets of collocation points within the meshes of this domain are Legendre-Gauss (LG), Legendre-Gauss-Radau (LGR), and Legendre-Gauss-Lobatto (LGL) points. LG points do not include either the initial or terminal endpoints of the mesh, LGR points include only one endpoint (either the initial or terminal), and LGL points include both of the endpoints.

Rao et al. developed a Matrix Laboratory (MATLAB) software called GPOPS-II, which utilizes pseudospectral methods and sparse nonlinear programming to solve multi-phase optimal control problems [19]. In multi-phase problems, each phase has its own cost function, dynamic constraints, and path constraints. Consequently, it is possible to divide a problem into multiple phases if the dynamics or constraints on the problem are not constant. The phases are connected together using linkage constraints, which prevent any discontinuities between phases for the states and controls. GPOPS-II employs an *hp*-adaptive Gaussian quadrature collocation method to achieve solution convergence at LGR points. h methods reach convergence by increasing the number of intervals, while p methods reach convergence by increasing the degree of the approximating polynomial. *hp*-adaptive methods combine h and p methods for convergence. The *hp*-adaptive methods allow for variance in the number and size of meshes as well as the degree of the approximating polynomial. This facilitates spectral convergence in regions where the solution is smooth and the introduction of additional mesh points in regions where the solution is discontinuous or changes rapidly [19]. GPOPS-II then employs sparse derivative approximations with a selected NLP solver, such as SNOPT or IPOPT.

2.4 Modeling Helicopter Descent With Optimal Control

In 1977, Johnson [4] applied optimal control theory to analyze the descent of a helicopter following power loss during level flight. Johnson's goal was to find the op-

timal control to land a helicopter with minimum velocity after losing power. Johnson modeled the helicopter as a point-mass whose motion stayed within a two-dimensional plane according to the force diagram in Figure 2.2. When formulating this optimal control problem, Johnson decided to use height above the ground as the independent variable instead of time, since the final height of the helicopter is known for the landing problem. The control variables for this model were the coefficient of thrust, C_T, and the angle of the thrust vector to the vertical, α. The collective pitch control could be determined from these control variables using blade element theory. The longitudinal cyclic pitch could not be determined from α without considering the helicopter's pitch attitude and rotor flapping, which Johnson did not include in this analysis. Following the simulated power shut-off, Johnson used nondimensional, non-linear equations of motion for the vertical descent velocity, horizontal velocity, rotor speed, and induced velocity as the differential equation constraints for the control problem. This model accounted for ground effect, rotor stall, vortex ring state, an exponential lag in the power drop of the engine following shut-off, and a time delay from the pilot's reaction time. A quadratic cost function was implemented to minimize both the vertical and horizontal velocities of the helicopter at landing. The boundary conditions were derived from the initial and final heights. Johnson applied the steepest descent algorithm, which is described in [13] and [17], to solve the two-point boundary value problem from the indirect method to solve this two-point boundary-value problem. The resulting solutions were in general agreement with available flight test data but did have some discrepancies, such as the initial behavior of the rotor speed following power loss. Johnson's analysis demonstrated that optimal control could effectively be adapted to evaluate the trajectory of a helicopter during autorotation.

In 1985, Lee [21] developed a point-mass dynamic model similar to the one used by Johnson. After incorporating the helicopter properties for an OH-58A helicopter

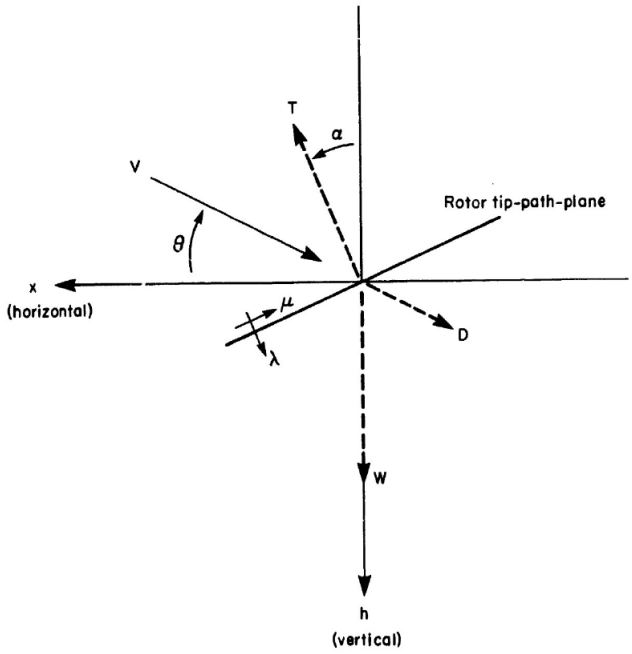

Figure 2.2. Force Diagram used by Johnson [4]

into the model, Lee formulated the optimal control problem to minimize the landing velocity. Along with initial and terminal boundary constraints, Lee included a path constraint to account for the limitations caused by blade stall. Lee solved the optimization problem for several different initial heights and airspeeds using the Sequential Gradient Restoration (SGR) algorithm. Lee's problem formulation assumed an instantaneous, total power loss and did not account for a reaction delay by the pilot. Among the notable conclusions reached during this research was the adequacy of a point-mass model in accurately representing the descent of a helicopter during autorotation. Lee found that the calculated point-mass steady-state sink rates were within the bounds of experimentally determined data from OH-58A flight tests. Thus, the pitching motion excluded from this model was determined to be negligible. Furthermore, the flight trajectories of the optimal solutions closely matched the flight tests. Lee also concluded that additional path constraints should be added for both the state and control variables to better reflect reality.

2.5 Optimal Control Analysis of OEI Flight

In the 1990's, Chen and Zhao investigated optimal trajectories for twin engine helicopters operating in one engine inoperable (OEI) flight [22]. Similarly to previous research, Chen and Zhao developed a two-dimensional, point-mass helicopter model. Unlike other models designed to analyze full power loss, their model included an additional state to account for the power supplied by the remaining operating engine after entering into OEI flight. Chen and Zhao implemented the SGR algorithm to determine the optimal trajectories during a rejected takeoff, continued takeoff, balked landing, and continued landing. One of the notable conclusions that Chen and Zhao reached was that ground effect has a significant effect in trajectory optimization for Vertical Takeoff and Landing (VTOL) flight.

In 2003, Carlson [23] collaborated with Zhao to apply optimal control theory to develop OEI HV diagrams for the XV-15 tiltrotor aircraft. One major differentiator between this and prior research was that Carlson employed direct collocation and NLP to solve the optimal control problem to determine points along the deadman's curve. The collocation method proved to be an improvement over many of the previous methods utilized for HV analysis.

Bachelder et al. [24] adapted a similar direct collocation optimal control strategy for analyzing OEI flight for the MH-60S and the CH-53D. Using the optimal trajectories, Bachelder estimated the high hover point and knee point of the HV curve. The results were compared to Sikorsky's method for examining HV diagrams with its HDP program. While the solutions were similar, the dynamic model used in the optimal control formulation was determined to be less accurate than the HDP dynamic model.

2.6 HV Diagram Determined Using GPOPS-II

In 2018, Harris [2] applied optimal control to analytically derive an OEI HV diagram for an AH-1Z helicopter. Harris developed a point-mass dynamic model that compared favorably to AH-1Z flight test data for low-speed flight. The optimal control problem formulation included constraints on the initial and final states as well as path constraints. Both the initial altitude of the helicopter and the final time were chosen to be free variables. Harris selected the cost function to minimize the initial altitude when finding points along the upper portion of the HV curve, and to maximize the initial altitude when finding points along the lower portion of the curve. Harris solved the optimal control problem using pseudospectral collocation via the GPOPS-II software discussed in Section 2.3.6. Based on the solutions at multiple conditions, Harris constructed an HV diagram. The research conducted during this thesis is a continuation of the work performed by Harris.

2.7 Autorotative Performance

A helicopter's autorotative performance relies on several factors, including rotor disk loading, stored kinetic energy, and blade loading. In Section 8.5 of [7], Johnson describes several performance indices based on some of these factors. These indices are useful in the design process of a helicopter to help ensure certain autorotative characteristics will be achieved as well as in analyzing the autorotative characteristics of existing rotorcraft. The development of many of these autorotation indices is summarized in [25]. The first index is the rotor energy factor, which is the kinetic energy of the main rotor divided by the helicopter's gross weight. The autorotation landing index represents the amount of time that touchdown can be delayed. This measure is dependent on rotor inertia and blade stall characteristics. The next autorotative index discussed by Wood is a measure of the usable energy level of the

helicopter, which depends on the operating and maximum blade loading coefficients. The last index is simply denoted autorotation index (AI) and is the ratio of the kinetic energy of the main rotor to the hover power required. Fradenburgh [26] introduced an additional autorotation measure, the flare index, which was used by Sikorsky Aircraft. The flare index is the ratio of the rotor energy available to energy required to perform the flare maneuver. Fradenburgh found a high correlation with this flare index and pilot opinion on the ease of landing during autorotation. In Chapter 5 of [27], Leishman compares the flare indices for several helicopters.

2.8 Conclusions from Previous Research

Initial approaches for constructing Height-Velocity diagrams revealed a need to supplement flight tests with accurate analytical methods. The first step in developing these analytical methods involves constructing a mathematical model representative of a helicopter's behavior during flight. Several studies have shown that a point-mass dynamic model can adequately portray a helicopter in autorotation. Optimal control has been successfully utilized to determine flight trajectories and estimate the boundary between safe and unsafe flight regions in the case of engine failure. Direct collocation methods in particular have proven to be effective in solving for the HV curve. The research reviewed in this chapter was fundamental in establishing the research methodology for this thesis as discussed in Chapter 3.

III. Research Methodology

3.1 Chapter Overview

This chapter describes the development of a helicopter dynamic model and the research methods employed to analyze varying effects on a helicopter's autorotation characteristics based on this model. The research approach for this thesis begins by developing a helicopter model based on previous research. That model is then incorporated into an optimal control problem to construct a Height-Velocity (HV) diagram. The optimal control formulation diverges from prior research by implementing an alternative method for determining the HV curve. Following the construction of the HV curve, the influence of ground effect in the dynamic model is investigated. Finally, additional factors affecting autorotation are analyzed.

3.2 Basic Assumptions

A point-mass model has been selected for this research since point-mass models have been shown by several studies, including those by Johnson [4] and Lee [21], to adequately represent a helicopter during flight. Since a helicopter ideally experiences minimal lateral movement when performing an autorotation, the model confines helicopter motion within a vertical plane. Similar to Harris's research [2], the rotor inflow is modeled using momentum theory and is assumed to be uniform. The helicopter mass is assumed to be constant throughout the autorotation, since any changes in mass due to factors such as fuel burn are negligible. The helicopter model reflects standard sea-level atmospheric conditions with no wind and constant air density. This research focuses on the low-speed portion of the HV diagram, thus assuming a low advance ratio. The engine failure occurs when the helicopter is in level, steady-state flight, which is often the assumed initial conditions for an HV diagram.

3.3 7-State Dynamic Model

3.3.1 Helicopter Model

The helicopter dynamic models used by Lee [21] and Harris [2] formed the starting point for the development of the models used in this research. The force diagram shown in Figure 3.1 depicts a point-mass helicopter in descent and provides the basis for the dynamic model's equations of motion. Balancing the vertical and horizontal forces acting on the point-mass produces Equations 3.1a and 3.1b, respectively.

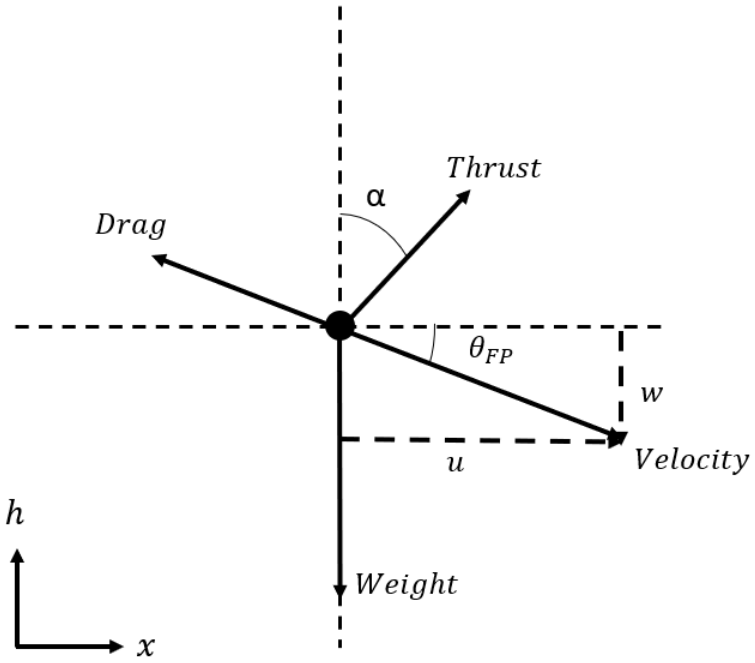

Figure 3.1. Point-Mass Helicopter Force Diagram

$$m\dot{w} = mg - T\cos\alpha - D\sin\theta \tag{3.1a}$$

$$m\dot{u} = T\sin\alpha - D\cos\theta \tag{3.1b}$$

Figure 3.1 also presents many of the state and control variables for the dynamic

model. The two controls are the rotor thrust and the angle of attack of the rotor disk plane, α. Two of the states describe the position of the helicopter: h is the height of the helicopter above the ground, and x is the horizontal distance the helicopter travels starting at engine failure. The next two states are the vertical and horizontal velocities of the helicopter, w and u, respectively. By definition, the derivatives of the positions are the velocities as shown in Equations 3.2a and 3.2b. It is important to note that a negative is included in Equation 3.2a, since the height is defined as positive in the upward direction, and the vertical velocity is defined as positive in the downward direction.

$$\dot{h} = -w \tag{3.2a}$$

$$\dot{x} = u \tag{3.2b}$$

The torque balance equation is given in Equation 3.3a, where the required torque is determined from Equation 3.3b. The torque coefficient is equivalent to the power coefficient, which is discussed in the next section. The energy balance equation for the helicopter rotor is shown in Equation 3.3d. These equations introduce another state variable in the rotor rotational speed, Ω.

$$I_R\dot{\Omega} = -Q_{Req} \tag{3.3a}$$

$$Q_{Req} = \rho A(\omega R)^2 C_Q \tag{3.3b}$$

$$C_Q = C_P \tag{3.3c}$$

$$I_R\Omega\dot{\Omega} = P_S - P_R \tag{3.3d}$$

3.3.2 Required Power

The total power required by the helicopter can be calculated as a combination of main rotor power, tail rotor power, and accessory power losses. After including the gearbox efficiencies, this summation becomes:

$$P_R = \frac{1}{\eta_C}\left(\frac{P_{MR}}{\eta_{MR}} + \frac{P_{TR}}{\eta_{TR}} + P_{Acc}\right) \tag{3.4}$$

The power requirements for the main rotor are calculated using the methods discussed in Section 6.4 of [7]. Johnson explains that the required rotor power for a helicopter in forward flight can be estimated by aggregating the rotor induced power, profile power, parasite power, and climb power. Equation 3.6 shows this relationship in terms of power coefficients.

$$P_{MR} = \rho A(\Omega R)^3 C_{P_{MR}} \tag{3.5}$$

$$C_{P_{MR}} = C_{P_i} + C_{P_o} + C_{P_P} + C_{P_C} \tag{3.6}$$

The rotor induced power is the power that is associated with the production of thrust. The calculation for the induced power coefficient, C_{P_i}, includes an empirical correction factor, k_i to account for any losses such as those from tip loss or nonuniform inflow.

$$C_{P_i} = k_i \lambda_i C_T \tag{3.7}$$

The profile power is the power necessary for the rotor blades to rotate through the air. The profile power coefficient, C_{P_o}, incorporates the average blade drag coefficient, c_{do}, and the helicopter speed as represented by the advance ratio, μ. The following

approximation is accurate for low advance ratios, such as those that are encountered during this research.

$$\mu = \frac{u \cos \alpha + w \sin \alpha}{\Omega R} \tag{3.8}$$

$$C_{P_o} = \frac{\sigma c_{do}}{8}(1 + 4.65\mu^2) \tag{3.9}$$

Whereas the profile power accounts for blade drag, rotor parasite power encompasses the drag from the whole helicopter. The drag that the helicopter experiences is estimated using an equivalent flat plate area, f, when calculating the profile power coefficient, C_{P_p}.

$$C_{P_p} = \frac{f}{2A}\mu^3 \tag{3.10}$$

The climb power is the power necessary for the helicopter to change its altitude. The climb power coefficient, C_{P_c}, is derived from the helicopter's vertical velocity, w, and the aircraft weight, W.

$$C_{P_c} = -\frac{wW}{\rho A(\Omega R)^3} \tag{3.11}$$

The purpose of the tail rotor is to balance the torque created by the main rotor and provide yaw control for the helicopter. As a result of having a longer moment arm, the tail rotor does not need to match the thrust produced by the main rotor and consequently has much lower power requirements than the main rotor. Rather than analyzing each of the components of power for the tail rotor, the required power for the tail rotor is calculated based on the thrust required to balance the main rotor torque. The following equation for tail rotor power used by Harris in [2] additionally

incorporates the advance ratio.

$$T_{TR} = \frac{Q_{MR}}{l_{TR}} \tag{3.12a}$$

$$C_{T_{TR}} = \frac{T_{TR}}{\rho A_{TR}(\Omega_{TR} R_{TR})^2} \tag{3.12b}$$

$$P_{R_{TR}} = (1 - 1.2\mu)\frac{C_{T_{TR}}}{M_{TR}} \tag{3.12c}$$

Accessory power losses are unique to each aircraft. Harris [2] provides empirically derived values for the accessory power losses for the AH-1Z.

3.3.3 Engine Power

Since this model is designed to analyze twin-engine rotorcraft during one engine inoperable (OEI) operations, the power provided to the rotor system by each engine is considered separately as individual state variables. P_1 denotes the power available from the engine that experiences failure. Immediately following the engine failure, the power available decays as shown in Equation 3.13 [28], where τ_1 is a time constant for the first engine.

$$\dot{P}_1 = -\frac{1}{\tau_1} P_1 \tag{3.13}$$

After losing power from the first engine, the second engine will increase its power output, P_2, to try to compensate for the loss. Equation 3.14b describes this increase in power output [22],[2]. The engine two time constant, τ_2 is used to calculate the rate of change for the power. There will naturally be a lag in the time it takes for the system to realize the working engine needs to compensate for the failed one, so the power output from the working engine will not immediately increase as shown in Equation 3.14a. Equation 3.14c describes the power available from the operating

engine after being modified by the engine governor [24]. The maximum power output for the single operating engine is given by P_{OEI}.

$$\dot{P}_2 = 0 \text{ for } t \leq 0.5 \tag{3.14a}$$

$$\dot{P}_2 = \frac{1}{\tau_2}(P_{2AG} - P_2) \text{ for } t > 0.5 \tag{3.14b}$$

$$P_{2AG} = min[P_{OEI}, P_R - G(\Omega - \Omega_0)] \tag{3.14c}$$

3.3.4 Rotor Inflow

Due to the descending flight path of helicopters during autorotation, the rotor will likely operate in vortex ring state (VRS). In [4], Johnson describes an algorithm using an empirical extension of momentum theory to determine rotor inflow during flight that encounters VRS. This algorithm uses the ideal induced velocity in hover, which is shown in Equation 3.15a, to find the rotor axial and radial velocity ratios as shown in Equation 3.15b and 3.15c. The velocity ratios are then input into the VRS model given by Johnson to estimate the inflow ratio, λ.

$$v_h = \sqrt{\frac{T}{2}} \tag{3.15a}$$

$$\mu_x = \frac{u\cos\alpha - w\sin\alpha}{v_h} \tag{3.15b}$$

$$\mu_z = \frac{u\sin\alpha - w\cos\alpha}{v_h} \tag{3.15c}$$

3.3.5 Ground Effect

Whenever a helicopter is in close proximity to the ground, the induced velocity at the rotor decreases. This phenomenon, known as ground effect, causes a reduction

in the amount of power required to produce a given thrust. Likewise, ground effect causes an increase in the amount of thrust produced by a rotor at a given power. Ground effect can be modeled by including a ground effect factor, k_g, to scale thrust. Equations 3.1a and 3.1b can then be modified as shown in Equations 3.23a and 3.23b to include this factor.

$$m\dot{w} = mg - Tk_g \cos\alpha - D\sin\theta \tag{3.16a}$$

$$m\dot{u} = Tk_g \sin\alpha - D\cos\theta \tag{3.16b}$$

There are several empirical models for determining what value to use for the ground effect factor. Section 4.8 of [7] lists six such models that are analyzed in this research. Equations 3.17-3.22 denote the ground effect models. The ground effect factor in the first three models is only a function of the rotor height above the ground, z, and the rotor radius. The last three models additionally use blade element theory to include rotor thrust into the calculations.

Cheeseman and Bennett:

$$k_g = \left[1 - \frac{1}{(4z/R)^2}\right]^{-1} \tag{3.17}$$

Hayden:

$$k_g = \left[0.9926 + \frac{0.03794}{(z/2R)^2}\right]^{2/3} \tag{3.18}$$

Schmaus, Berry, Gross, and Koliais:

$$k_g = \left[0.146 + 2.090\left(\frac{z}{R}\right) - 2.068\left(\frac{z}{R}\right)^2 + 0.932\left(\frac{z}{R}\right)^3 - 0.157\left(\frac{z}{R}\right)^4\right]^{-2/3} \tag{3.19}$$

The following ground effect models incorporate blade element theory:

Cheeseman and Bennett (blade element theory):

$$k_g = \left[1 + 1.5\frac{\sigma a \lambda_i}{4C_T}\frac{1}{(4z/R)^2}\right] \tag{3.20}$$

Law:

$$k_g = \left[\frac{1.0991 - 0.1042/(z/D)}{1 + (C_T/\sigma)(0.2894 - 0.3913/(z/D))}\right]^{-1} \tag{3.21}$$

Zbrozek:

$$k_g = \left[0.9122 + \frac{0.0544}{(z/R)\sqrt{C_T/\sigma}}\right] \tag{3.22}$$

Figure 3.2 compares the values for the ground effect factors for each of the above models as a function of z/R. For this comparison, the models incorporating blade element theory utilized values of thrust for hover. As z/R increases, the values for the ground effect factor approach one, since ground effect becomes negligible once the helicopter rotor is more than one rotor diameter above the ground. For the purposes of this study, the ground effect factor equals one whenever $z/R \geq 2$.

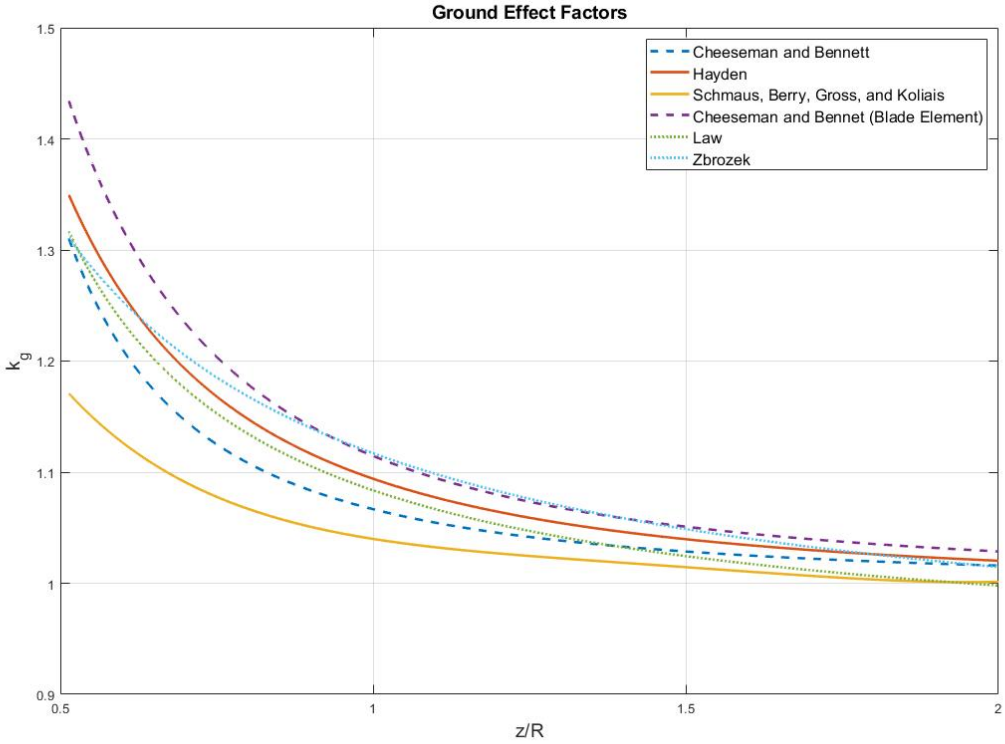

Figure 3.2. Comparison of Ground Effect Models

3.3.6 Equations of Motion

The seven dynamic equations described above that compose the equations of motion for this model are:

$$m\dot{w} = mg - Tk_g \cos\alpha - D\sin\theta \tag{3.23a}$$

$$m\dot{u} = Tk_g \sin\alpha - D\cos\theta \tag{3.23b}$$

$$I_R\dot{\Omega}\Omega = P_1 + P_2 - P_{Req} \tag{3.23c}$$

$$\dot{h} = -w \tag{3.23d}$$

$$\dot{x} = u \tag{3.23e}$$

$$\tau_1\dot{P}_{s1} = -P_{s1} \tag{3.23f}$$

$$\tau_2\dot{P}_2 = 0 \text{ for } t \leq 0.5 \tag{3.23g}$$

$$\tau_2\dot{P}_{s2} = P_{A2G} - P_{s2} \text{ for } t > 0.5 \tag{3.23h}$$

3.3.7 States

The seven state variables selected for this model are listed in Equations 3.24a-3.24g. Each of these states have been nondimensionalized to allow for ease of calculations in the dynamic model. The states have been scaled so that each variable is approximately the same order of magnitude. The scaling follows similar scaling

techniques used by Lee [21], Johnson [4].

$$x_1 = \frac{w}{0.01\Omega_0 R} \tag{3.24a}$$

$$x_2 = \frac{u}{0.01\Omega_0 R} \tag{3.24b}$$

$$x_3 = \frac{\Omega}{\Omega_0} \tag{3.24c}$$

$$x_4 = \frac{h}{10R} \tag{3.24d}$$

$$x_5 = \frac{x}{10R} \tag{3.24e}$$

$$x_6 = \frac{P_1}{P_{OEI}} \tag{3.24f}$$

$$x_7 = \frac{P_2}{P_{OEI}} \tag{3.24g}$$

3.3.8 Controls

The two control variables are the thrust coefficient and the angle of attack of the rotor tip path plane.

$$u_1 = 1000 C_T \tag{3.25a}$$

$$u_2 = \alpha \tag{3.25b}$$

3.3.9 Nondimensional Equations of Motion

In order to nondimensionalize each of the variables in the dynamic model, time must also be addressed. Lee [21] uses the following equations to define nondimensional time, τ, and the derivative with respect to that non-dimensional time, which

is denoted in the equations of motion using a prime notation (').

$$\tau = \frac{t}{t_{ref}} \tag{3.26a}$$

$$t_{ref} = \frac{100}{\Omega_0} \tag{3.26b}$$

$$\tau = \frac{\Omega_0 t}{100} \tag{3.26c}$$

$$\frac{d}{d\tau} = \frac{100}{\Omega_0}\frac{d}{dt} \tag{3.26d}$$

Incorporating all of the nondimensional terms into the dynamic equations produces the following equations of motion:

$$x_1' = g_0 - m_0 x_3^2 k_g u_1 \cos u_2 - f_{0z} x_1 \sqrt{x_1^2 + x_2^2} \tag{3.27a}$$

$$x_2' = m_0 x_3^2 k_g u_1 \sin u_2 - f_{0x} x_2 \sqrt{x_1^2 + x_2^2} \tag{3.27b}$$

$$x_3' = \frac{i_0}{x_3}\left(x_6 + x_7 - P_{R1}\right) \tag{3.27c}$$

$$x_4' = -0.1 x_1 \tag{3.27d}$$

$$x_5' = 0.1 x_2 \tag{3.27e}$$

$$x_6' = -k_1 x_6 \tag{3.27f}$$

$$x_7' = 0 \text{ for } \tau \leq \frac{0.5}{t_{ref}} \tag{3.27g}$$

$$x_7' = k_2(P_2 - x_7) \text{ for } \tau > \frac{0.5}{t_{ref}} \tag{3.27h}$$

3.3.10 Additional Parameters

Additional nondimensional variables for the power terms that are included in the equations of motion are:

$$P_{R1} = \frac{P_R}{P_{OEI}} \tag{3.28a}$$

$$P_2 = min[P_{R1} - G_1(x_3 - 1), 1] \tag{3.28b}$$

The constants used in this dynamic model are:

$$g_0 = \frac{10,000g}{\Omega_0^2 R} \tag{3.29a}$$

$$m_0 = \frac{10\rho\pi R^3}{m} \tag{3.29b}$$

$$f_{0_z} = \frac{\rho f_{e_z} R}{2m} \tag{3.29c}$$

$$f_{0_x} = \frac{\rho f_{e_x} R}{2m} \tag{3.29d}$$

$$i_0 = \frac{100 P_{OEI}}{I_R \Omega_0^3} \tag{3.29e}$$

$$k_1 = \frac{t_{ref}}{\tau_1} \tag{3.29f}$$

$$k_2 = \frac{t_{ref}}{\tau_2} \tag{3.29g}$$

$$G_1 = \frac{G\Omega_0}{P_{OEI}} \tag{3.29h}$$

3.4 Optimal Control Problem Formulation

The optimal control problem for this research implements the above helicopter model to determine minimum landing velocities for a grid of initial altitudes and airspeeds. A HV diagram can then be delineated based on the resulting solutions.

The equations of motion of the helicopter serve as equality constraints in the optimal control problem. The initial conditions, path constraints, and final conditions provide additional equality and inequality constraints.

3.4.1 Optimal Control Problem Statement

The initial cost function selected for this research was simply the square root of the sum of the final landing velocities squared. The cost function was then weighted in order to minimize the vertical landing velocity more than the landing airspeed. This weighting reflects the requirement of a lower vertical velocity to land safely. An inverse tangent of the two final velocities was also appended to the cost function to promote a vertical landing. This addition was found to improve convergence and generate better solutions for the upper portion of the HV curve.

$$\begin{aligned} \underset{u}{\text{minimize}} \quad & J = \sqrt{100x_{1f}^2 + x_{2f}^2} + \tan^{-1}\left(\frac{x_{2f}}{x_{1f}}\right) \\ \text{subject to} \quad & \mathbf{x}' - \mathbf{f} = 0, \\ & x(\tau_0) - x_0 = 0, \\ & g_1(x) \leq 0, \\ & g_2(u) \leq 0, \\ & x(\tau_f) - x_f = 0 \end{aligned} \tag{3.30}$$

A significant difference between this problem formulation and that of Harris [2] is the chosen cost function. Harris's cost function minimized or maximized the initial height given an initial airspeed and constraints on the final landing velocity. This cost function minimizes the landing velocity of the helicopter for a given set of initial conditions. Based on the solutions for the final velocities, a determination can be made whether a safe landing is possible from the given initial height and airspeed.

3.4.1.1 Initial Conditions

The initial conditions are based on the selected starting height and airspeed for the given iteration. Level flight is assumed at the instant of engine failure, so the initial vertical velocity is set equal to zero. The rotor angular velocity, thrust, power, and rotor angle of attack are calculated for the trim flight conditions for the chosen height and horizontal velocity.

$$
\begin{aligned}
t_0 &= 0 \\
w_0 &= 0 \\
u_0 &= \text{Selected initial airspeed} \\
\Omega_0 &= \text{Trim condition } \Omega \\
h_0 &= \text{Selected initial altitude} \\
x_0 &= 0 \\
P_{1_0} &= \text{Engine 1 power at engine failure} \\
P_{2_0} &= \text{Engine 2 power at engine failure} \\
C_{T_0} &= \text{Trim condition } C_T \\
\alpha_0 &= \text{Trim condition } \alpha
\end{aligned}
$$

3.4.1.2 Path Constraints

The states and controls are subject to the following path constraints:

$$
\begin{aligned}
0 \leq \ & t \ \leq t_{max} \\
0 \leq \ & w \ \leq w_{max} \\
0 \leq \ & u \ \leq u_{max} \\
\Omega_{min} \leq \ & \Omega \ \leq \Omega_{max} \\
0 \leq \ & h \ \leq h_0 \\
0 \leq \ & x \ \leq x_{max} \\
0 \leq \ & P_1 \ \leq P_{OEI} \\
0 \leq \ & P_2 \ \leq P_{OEI} \\
0 \leq \ & C_T \leq C_{Tmax} \\
\alpha_{min} \leq \ & \alpha \ \leq \alpha_{max}
\end{aligned}
$$

Many of the minimum and maximum bounds for the path constraints are chosen based on the helicopter properties and match the path constraints used by Harris in [2]. The maximum values for time and distance, x, were chosen to be values that are much larger than what would be achieved during an OEI autorotation.

$$
\begin{aligned}
t_{max} &= 15 * t_{ref} \\
w_{max} &= 3000 \tfrac{ft}{min} \\
u_{max} &= 200 kts \\
\Omega_{min} &= 0.92 * \Omega_0 \\
\Omega_{max} &= 1.06 * \Omega_0 \\
x_{max} &= 10000 ft \\
P_{OEI} &= 869,000 \tfrac{ft*lb}{sec} \\
C_{Tmax} &= 0.015 \\
\alpha_{min} &= -8 \deg \\
\alpha_{max} &= 8 \deg
\end{aligned}
$$

3.4.1.3 Final Conditions

Since the final condition describes the helicopter as it lands on the ground, the final altitude has an equality constraint set to zero.

$$h_f = 0$$

The remainder of the states and controls are not fixed but are still bounded by the path constraints listed above.

3.5 Methodology Summary

This chapter describes the research methodology used for this thesis. It outlines the equations of motion for the dynamic model as well as the optimal control problem formulation. The solution of the optimal control problem includes the minimum landing velocity that the helicopter has from a given set of initial conditions. The magnitude of the horizontal and vertical landing velocities determine if that test case is in the safe or unsafe region of flight. Compiling several test cases produces an HV diagram. This chapter also presents several ground effect models that will be incorporated into the overall helicopter dynamic model.

IV. Results

4.1 Chapter Overview

This chapter begins by discussing the optimal control solutions for the 7-state helicopter model. An Height-Velocity (HV) diagram is then presented based on these solutions. After establishing an initial HV diagram, changes are then made to the helicopter model to analyze the effects that various factors have on a helicopter's autorotation performance and HV diagram. Variations in the ground effect factor as well as changes to helicopter characteristics, such as gross weight and rotor radius, are presented.

4.2 7-State Helicopter Model Results

The baseline for the investigations composing this research uses the helicopter dynamic model and accompanying optimal control problem formulation discussed in Chapter 3 with the parameters of the AH-1Z as given in [2]. Solving the optimal control problem addresses whether the helicopter is able to safely land following an autorotation from a given initial flight condition. Compiling those answers for an array of test cases generates an HV diagram that displays the safe and unsafe regions of flight.

4.2.1 Flight Trajectories and Optimal Controls

4.2.1.1 Safe Region

Figure 4.1 shows the helicopter's trajectory following single-engine failure occurring at a height of 100 feet while flying at an airspeed of 10 knots. This trajectory follows the typical phases of an autorotation. The beginning of the flight path shows

a slight decrease in altitude as the main rotor stops receiving power from the failed engine. That is followed by a steady rate of descent as the helicopter flies forward. The rate of descent then levels out as the helicopter flares before touching down on the ground.

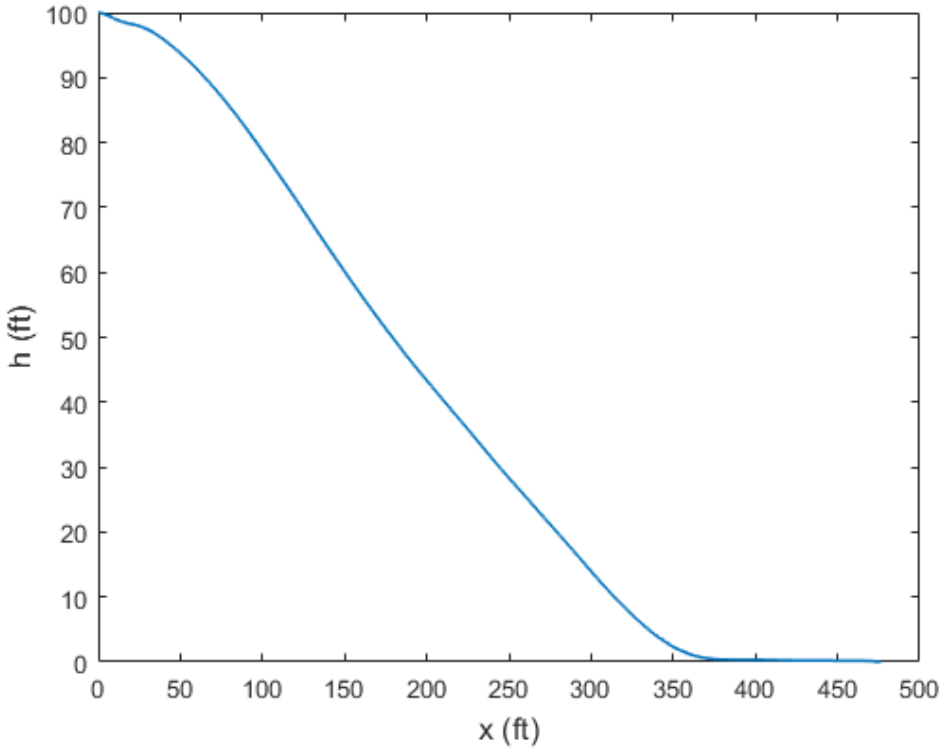

Figure 4.1. Autorotation Trajectory from an Airspeed of 10 Knots at 100 Feet

The time histories of each of the states and controls for this flight profile are presented in Figure 4.2. Once again, the helicopter's trajectory can be seen by the plots of the states h and x. Both the horizontal and vertical velocities increase during the first portion of the autorotation as the helicopter dives. They then plateau momentarily during the steady-state autorotation before decreasing as the helicopter flares as it approaches the ground. This test case represents a safe landing since both u and w reach zero velocity at landing. The helicopter begins steady-state autorotation around five seconds after engine failure, and then commences the flare approximately

nine seconds after engine failure. The rotor speed decreases initially after failure before slowly increasing during the steady-state descent. As the helicopter flares, the rotor speed decreases significantly as the helicopter slows down to land. As the power from the failed engine quickly decreases to zero after failure, the power output from the remaining engine increases to the one engine inoperable (OEI) power limit to attempt to compensate for the lost engine. There is a small delay of half a second for the power output from the remaining engine to increase. This lag represents the time it takes for the second engine to recognize that the first engine has failed. For the controls, the rotor tip-path-plane angle of attack starts at the upper limit before oscillating and decreasing to the lower limit. The rotor thrust increases sharply as the helicopter enters into a dive in the first second after engine failure. The thrust levels out during the steady-state autorotation phase before increasingly slightly when the helicopter flares. The thrust then decreases as the helicopter lands on the ground.

Figure 4.3 displays the profile for another safe landing. This test case started from hover at 20 feet. One key difference between this flight profile and the previous one from 100 feet is that the rotor speed increases initially rather than decreasing. This is a result of the compressed amount of time for an autorotation due to the engine failure occurring closer to the ground, which does not allow for a very long descent before the flare. The flare occurs shortly before two seconds after engine failure. During the flare, the rotor plane angle of attack decreases sharply while the thrust increases. Both the vertical and horizontal velocities decrease as a result, and the helicopter is able to land with zero velocity.

4.2.1.2 Hover Points

The low hover point and high hover point were determined by iteratively solving the optimal control problem at incremental initial altitudes in hover. Table 4.1

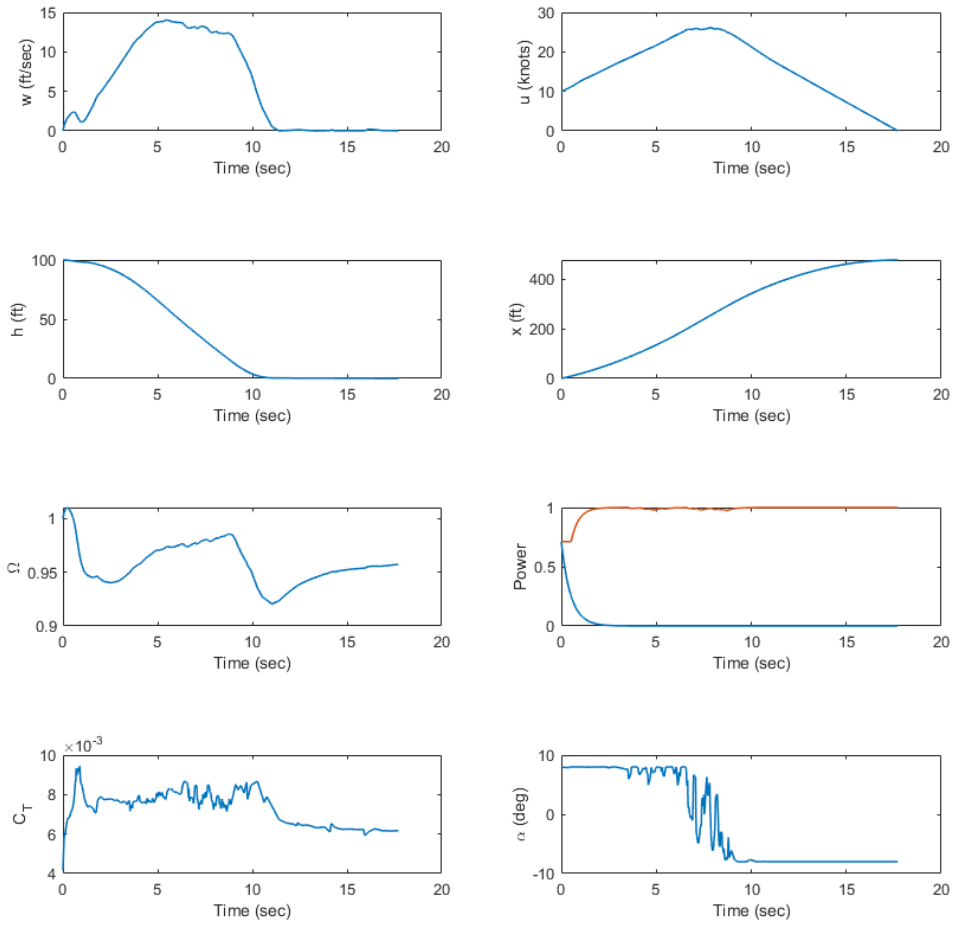

Figure 4.2. States and Controls for Autorotation from an Airspeed of 10 Kts at 100 Feet

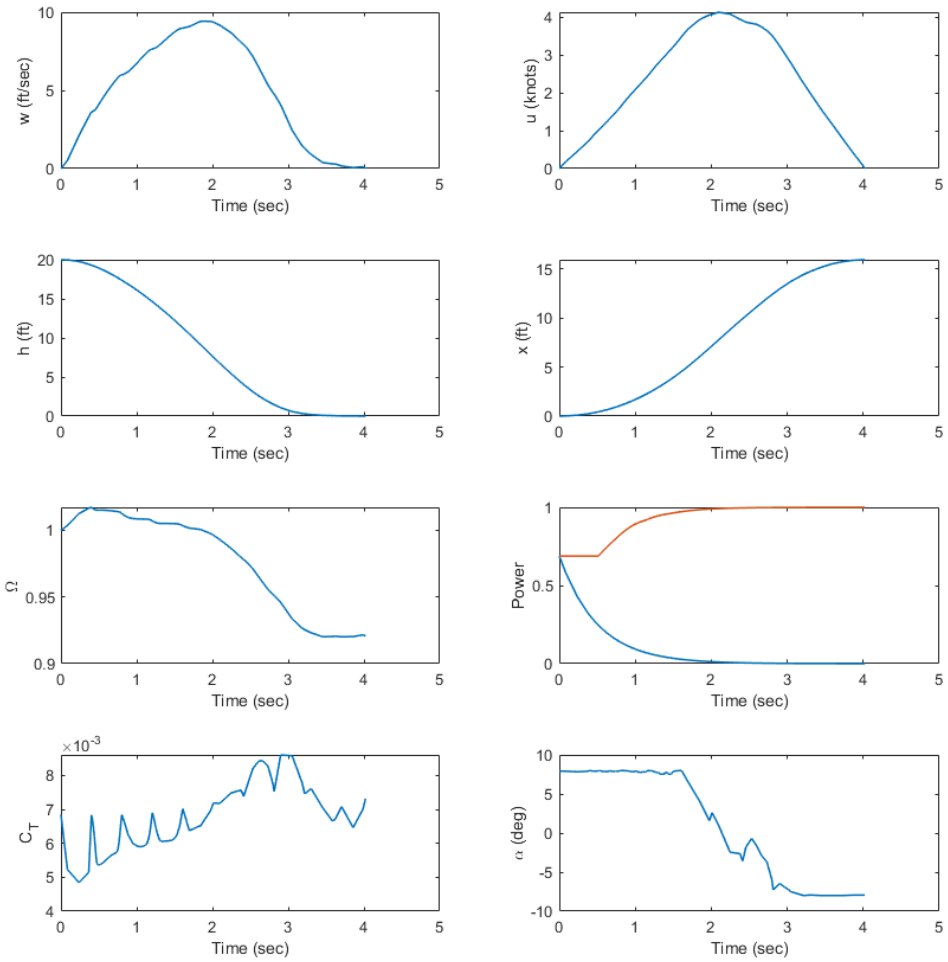

Figure 4.3. States and Controls for Autorotation from Hover at 20 Feet

presents the vertical and horizontal landing velocities for each initial height. The cutoff limits between a safe and unsafe landing were selected to be $w < 2.5$ ft/sec and $u < 10$ knots based on the structural limitations of the AH-1Z [2]. Accordingly, the low hover point is 39 feet and the high hover point is 151 feet.

Table 4.1. Altitude Sweep at Hover

h_0 **(ft)**	w_f **(ft/sec)**	u_f **(kts)**
200	0	0
180	0	0
170	0	0
160	0	0
155	0	0
151	0	0
150	0.5188	26.6797
140	1.8953	28.2395
130	6.5302	25.6929
120	8.9302	23.5834
110	10.6011	21.8575
100	11.8093	20.1867
90	12.2150	14.0673
80	8.4619	12.8871
70	9.9964	11.2041
60	8.3174	10.0912
50	6.2101	8.9857
40	3.5600	7.7777
39	2.3217	7.9593
38	2.0254	7.6686
35	2.0334	6.7792
30	1.0817	0.0000
25	0	0
20	0	0
10	0	0

Figures 4.4 and 4.5 show the associated states and controls for the low hover point and high hover point, respectively.

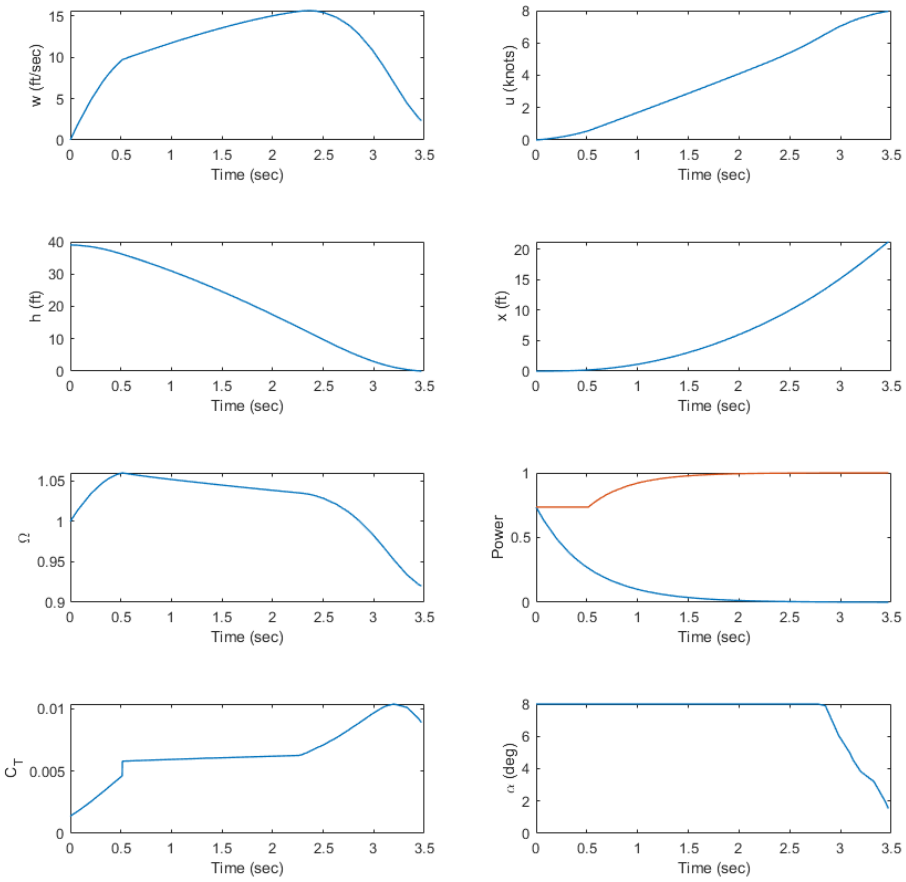

Figure 4.4. States and Controls for Autorotation from Hover at 39 Feet

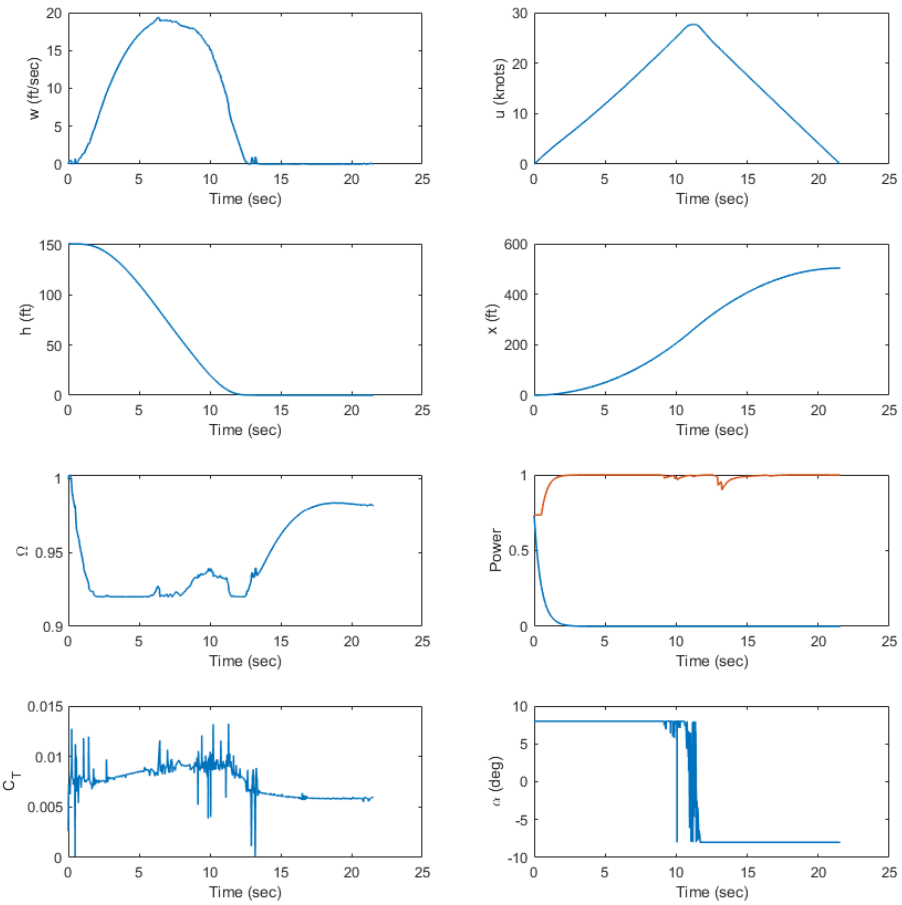

Figure 4.5. States and Controls for Autorotation from Hover at 151 Feet

4.2.1.3 Unsafe Region

Within the unsafe region of the HV envelope, the helicopter's velocity is unable to decrease sufficiently to allow for a safe landing. The states for the test case of four knots at 70 feet is shown in Figure 4.6. As can be seen, the helicopter's airspeed continues to increase throughout the autorotation until the aircraft impacts the ground. Meanwhile, the vertical velocity increases during the dive then decreases during the flare. This difference in behavior for the two velocities is a result of the selected objective function for the optimal control problem, which prioritizes reducing the vertical landing velocity more than the final airspeed. Weighting the landing velocities differently in the cost function would slightly alter the optimal control solution, but was not found to significantly change the location of the HV curve during this research. Since the horizontal velocity does not decrease during the flare, the helicopter is unable to land safely. As a result, this test case represents a point in the unsafe region of flight.

Figure 4.7 shows a comparison of the trajectories for autorotations from the two hover points and an initial airspeed of 4 knots at 70 feet. For the autorotation from the high hover point, the helicopter can be seen flaring above the ground as it slows down before landing. For the case with initial conditions of 4 knots at 70 feet, the helicopter starts a flare as it approaches the ground, but does not slow down enough to avoid crashing. The autorotation from the low hover point appears to follow a similar trajectory without much of a flare. The helicopter is still able to land safely though as a consequence of having less need for a large flare, since it is descending at a lower velocity.

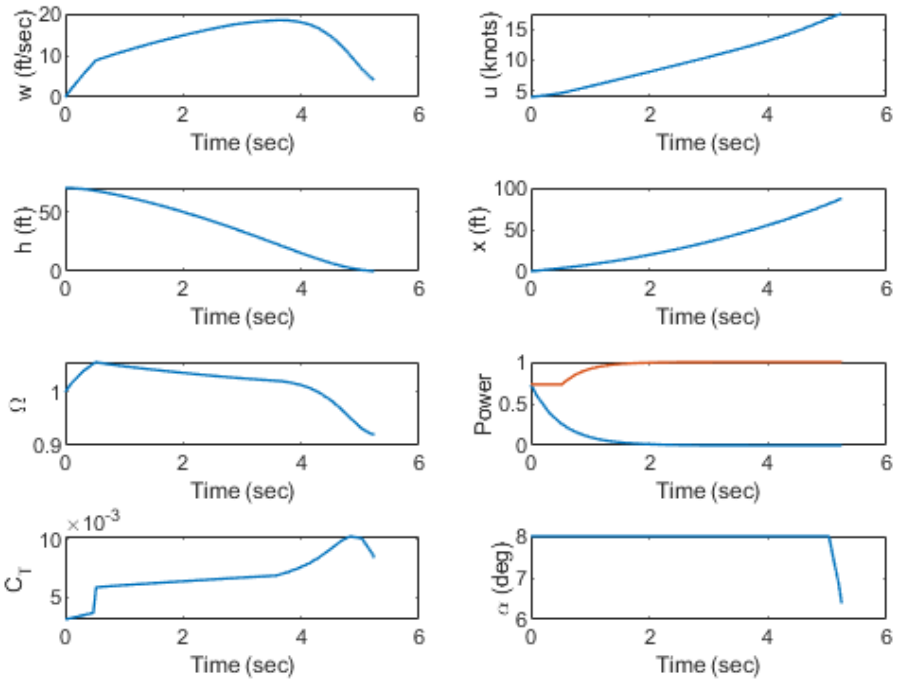

Figure 4.6. States and Controls for an Airspeed of 4 Knots at 70 Feet

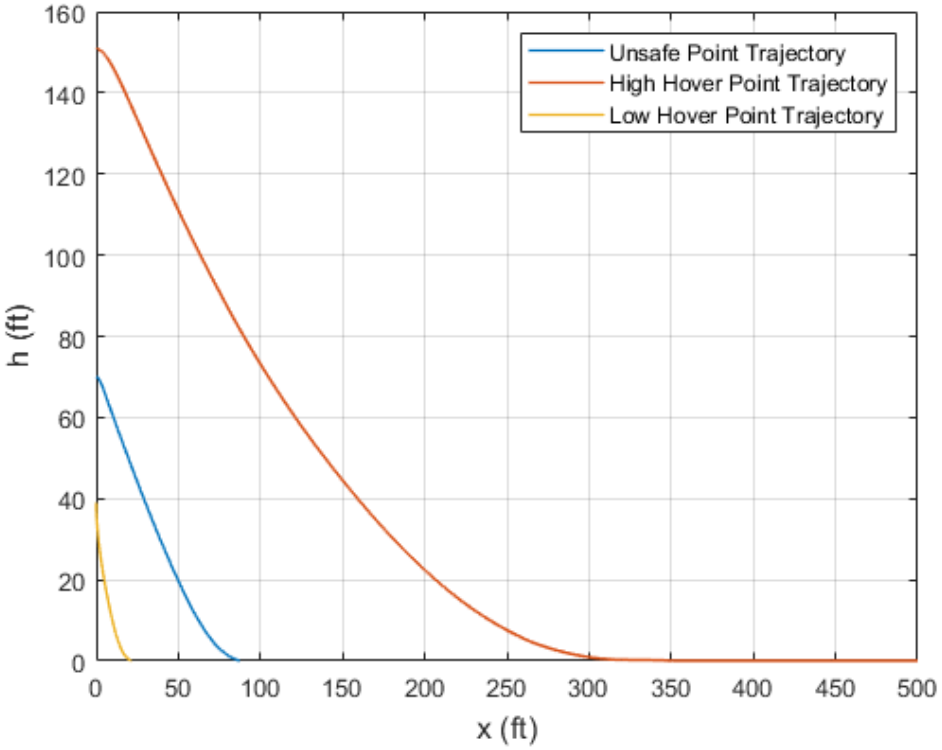

Figure 4.7. Autorotation Trajectories

4.2.2 Height-Velocity Diagram

The iterative process of incrementally adjusting the initial height was repeated at several airspeeds. This produced a grid of test cases at varying initial heights and airspeeds. The landing velocities for each of these test cases were compiled to construct the HV diagram in Figure 4.8. The green circles represent test cases in which the helicopter was able to land with both zero vertical and horizontal final velocities. The yellow circles are test cases in which the helicopter lands with nonzero velocities that are within the limits for a safe landing. The red points are the test cases that are within the unsafe flight envelope.

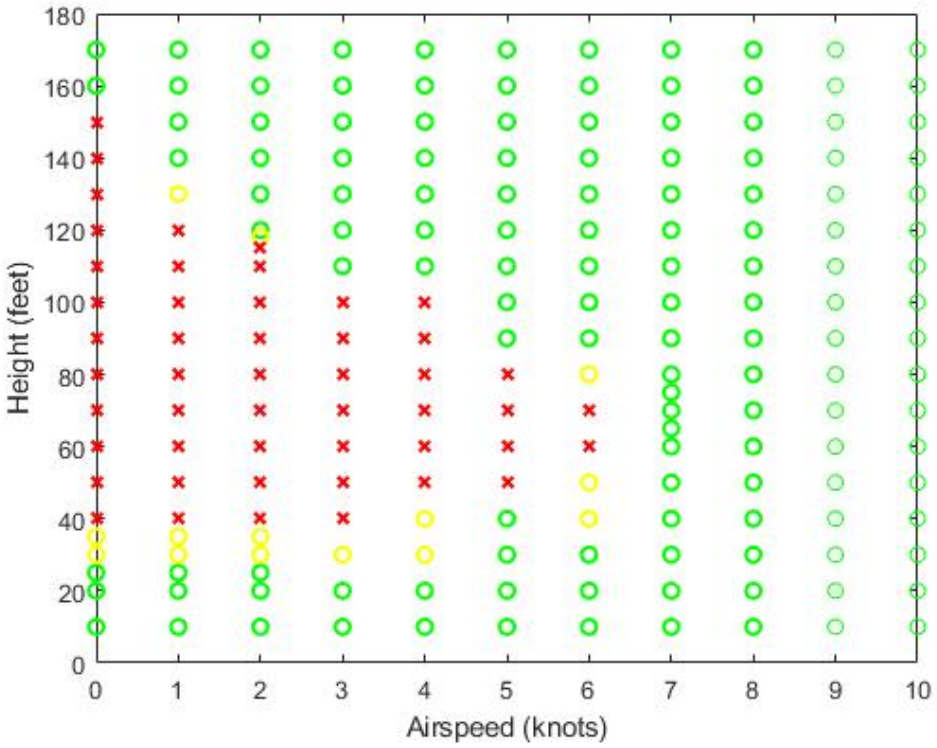

Figure 4.8. 7-State HV Diagram

This methodology for constructing an HV diagram provides the minimized landing velocities for each set of initial conditions. This allows for a full grid of safe and unsafe points to be compiled. In comparison, the methodology used by Harris [2]

only determined points along the HV curve by solving for the height at a given airspeed and landing velocity. That method encounters problems with the optimal control converging for certain test cases, especially near the knee point.

4.3 Ground Effect Investigation

The HV diagram above utilizes Hayden's method for calculating the ground effect factor. To investigate the influence of ground effect on the dynamic model, the other ground effect models discussed in Chapter 3 were implemented. In addition, test cases utilizing various percentages of the Hayden ground effect factor were analyzed.

4.3.1 Ground Effect Models

Five additional methods for calculating the ground effect factor were implemented into the helicopter's dynamic model. The optimal control solution process was used as above for an array of test cases to approximate the low hover point, high hover point, and knee point. Each of the resulting HV diagrams are shown in Figures 4.9-4.13.

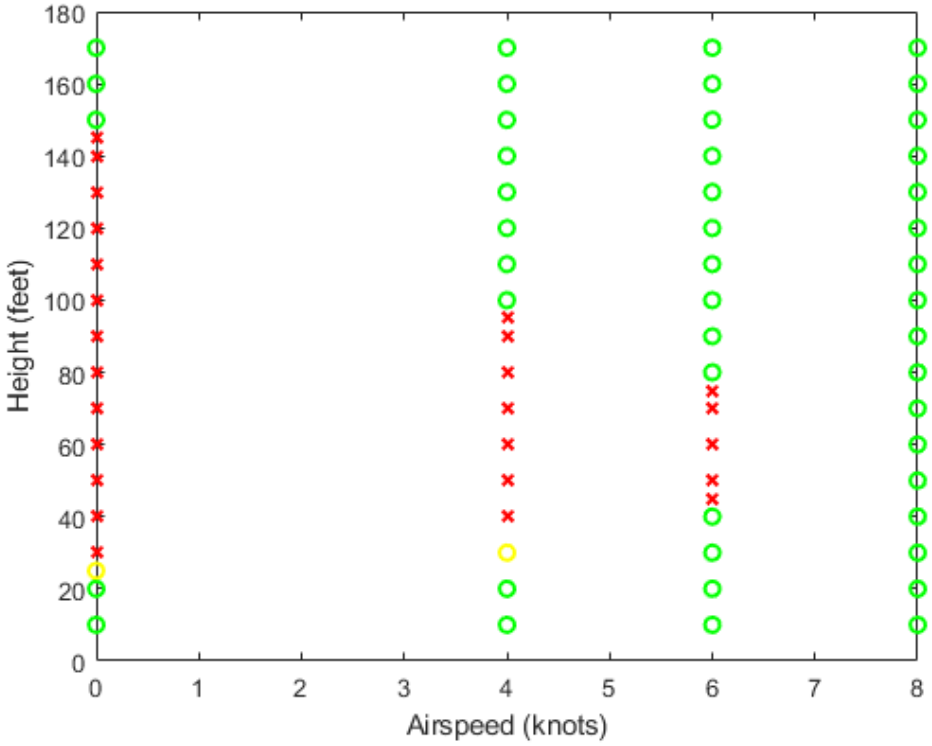

Figure 4.9. HV Diagram Using the Cheeseman/Bennett Ground Effect Factor

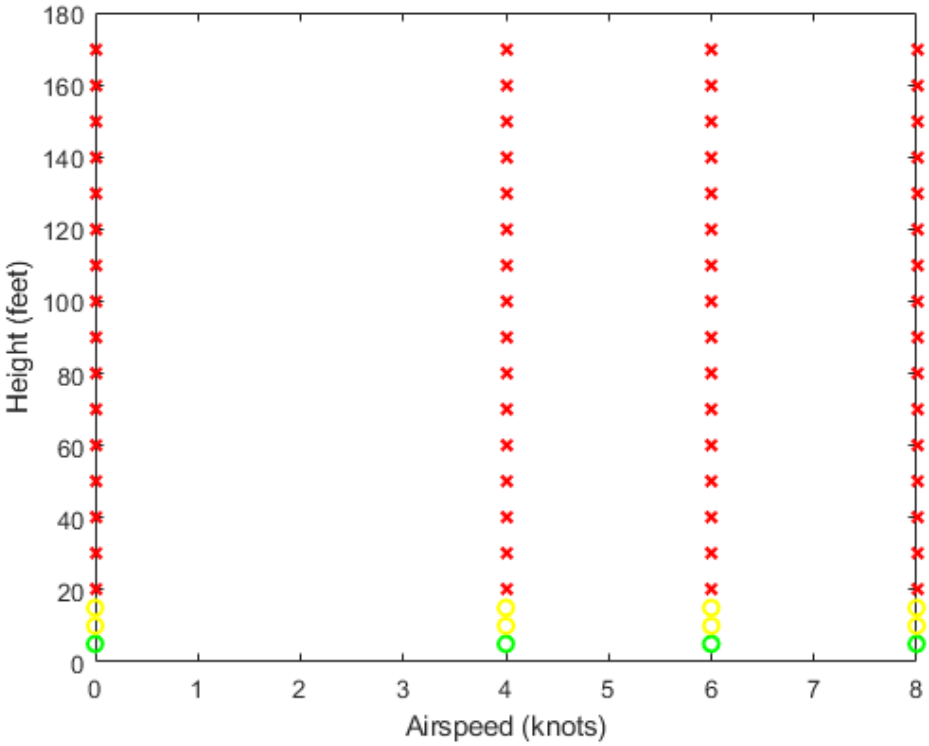

Figure 4.10. HV Diagram Using the Schmaus/Berry/Gross/Koliais Ground Effect Factor

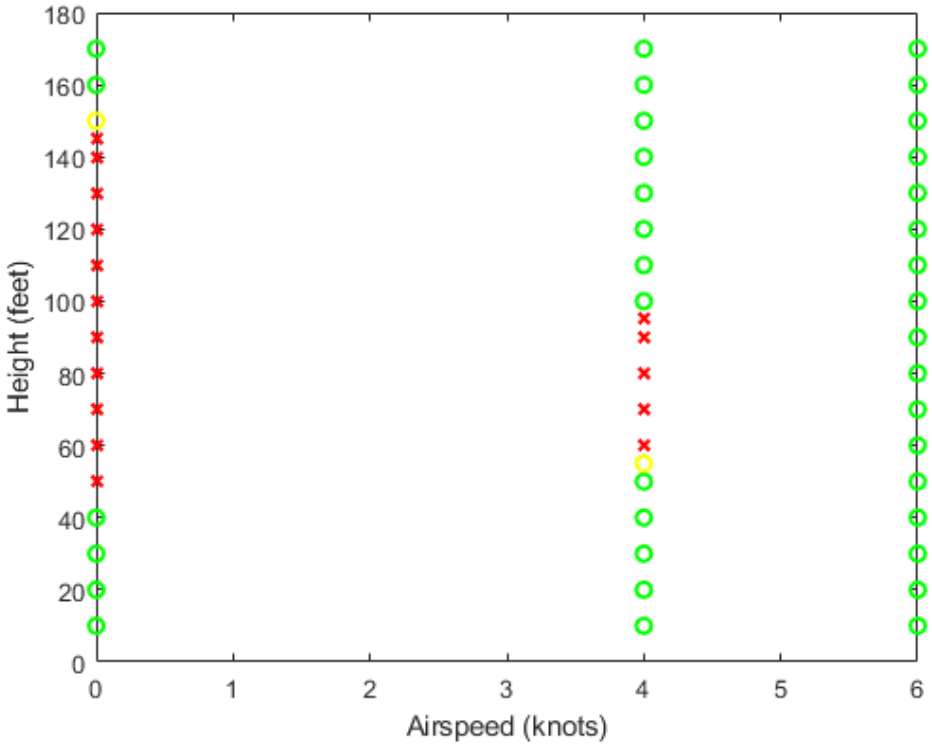

Figure 4.11. HV Diagram Using the Cheeseman/Bennett Blade Element Theory Ground Effect Factor

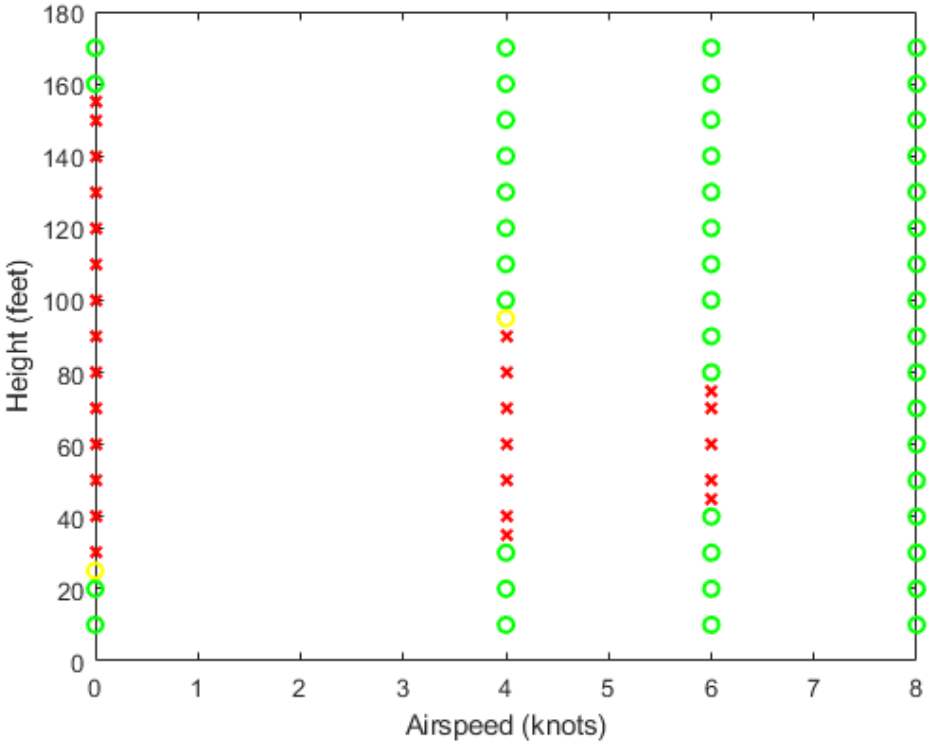

Figure 4.12. HV Diagram Using the Law Ground Effect Factor

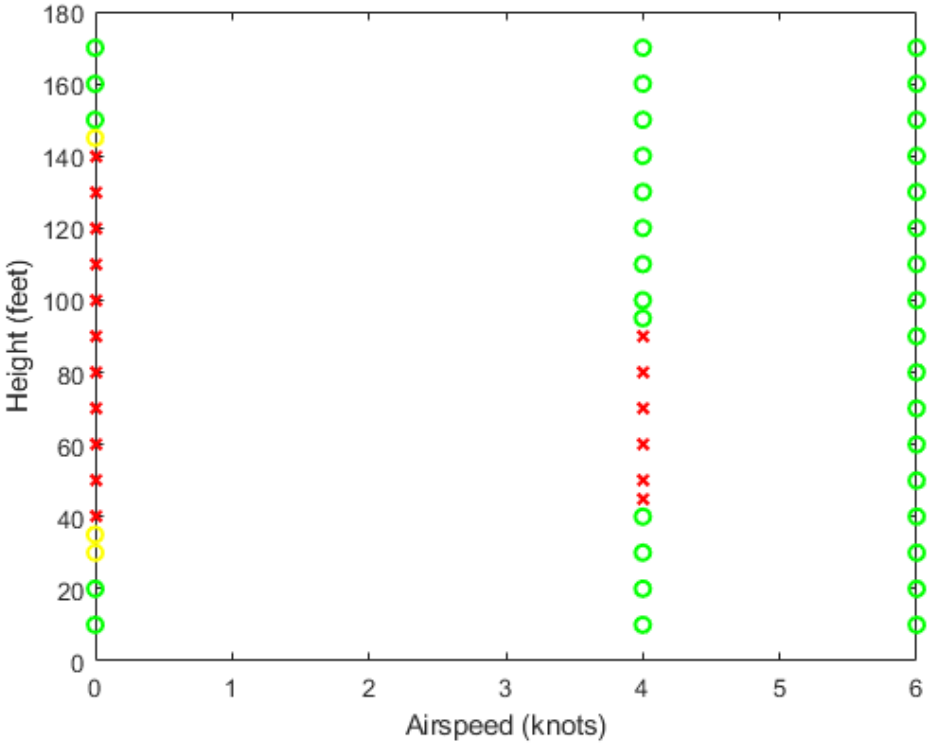

Figure 4.13. HV Diagram Using the Zbrozek Ground Effect Factor

Table 4.2 lists the low and high hover points determined from using each of the different ground effect models. The Cheeseman and Bennett model using blade element theory had the smallest HV envelope. This result was expected because that model has the largest ground effect factor as seen in Figure 3.2. A higher ground effect factor means that whenever the helicopter is near the ground, more thrust can be produced for a given power output. The helicopter can then flare more effectively, which allows it to land safely from a wider range of initial conditions. Contrastingly, having a lower ground effect factor in the dynamic model impedes the helicopter's flare performance. The model developed by Schmaus et al. provides the smallest ground effect factor of any of the methods analyzed in this research. As illustrated by Figure 4.10, an HV curve was not able to be defined using this ground effect model. While the optimal control solutions showed that the helicopter was able to land safely when beginning the autorotation at low initial heights, the lack of significant ground effect in the model made successful autorotations unachievable from above an initial height of approximately 20 feet. Several test cases were conducted at high initial altitudes up to 1000 feet as well as high initial airspeeds up to 40 knots without achieving landing velocities within the safe limits. Thus, no high hover point or knee point could be estimated using the Schmaus ground effect model.

Excluding the results from the Schmaus et al. model, the low hover points are between 29 feet and 49 feet, and the high hover points are between 144 feet and 156 feet. The knee points are all under an airspeed of 8 knots, and they are under 6 knots for both the Zbrozek and Cheeseman/Bennett blade element theory models. Figure 4.14 outlines points along the HV curve for each of ground effect models. (Note: Dashed lines between the points are shown to better see and compare the different models. The dashed lines do not accurately represent the shape of the HV curves.)

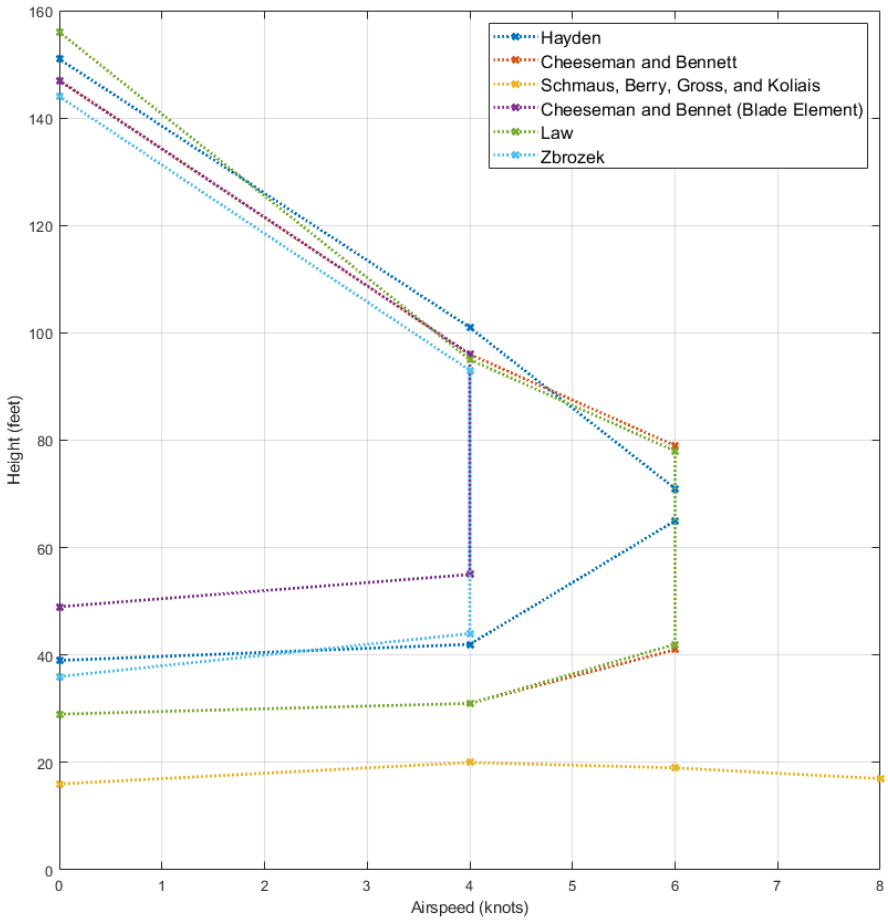

Figure 4.14. Comparison of Ground Effect Factors

Table 4.2. Hover Points for Each Ground Effect Model

Ground Effect Model	Low Hover Point (ft)	High Hover Point (ft)
Cheeseman and Bennett (BE)	49	147
Hayden	39	151
Zbrozek	36	144
Cheeseman and Bennett	29	147
Law	29	156
Schmaus, Berry, Gross, and Koliais	16	-

4.3.2 Variance of Ground Effect Factor

In conjunction with analyzing the six ground effect factor models, test cases were conducted using the Hayden ground effect factor reduced to 90%, 50%, 10%, and 0% of its nominal value. As expected, the reduction to 90% of the ground effect factor slightly increased the size of the unsafe flight region. The low hover point decreased by seven feet, while the high hover point remained approximately the same with a shift of one foot. Figure 4.15 presents a partial HV diagram for the 90% ground effect factor. The reduction to 50% of the ground effect factor produced similar results as the Schmaus model. The low hover point decreased by twenty-one feet. As with the Schmaus model, neither a high hover point nor a knee point could be determined. Further reductions to 10% and 0% (i.e. no ground effect) yielded similar results, except with the low hover point dropping below ten feet.

Table 4.3. Hover Points for Each Ground Effect Model

Percent of Ground Effect Factor	Low Hover Point (ft)	High Hover Point (ft)
100%	39	151
90%	32	150
50%	18	-
10%	8	-
0%	7	-

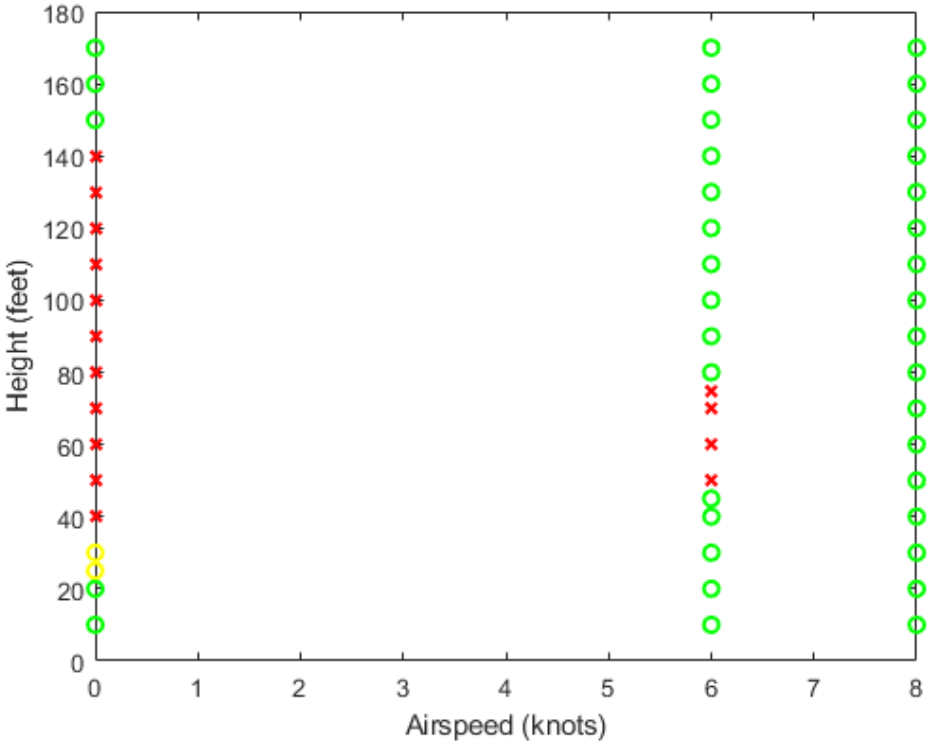

Figure 4.15. 90% Ground Effect Factor

4.4 Autorotation Index

A brief study was conducted to analyze the effect that changing helicopter characteristics, such as gross weight and main rotor radius, has on the helicopter's ability to land an autorotation safely. For each set of initial conditions, the helicopter parameters were set such that the helicopter could land with zero velocity. Individual parameters were then adjusted incrementally until the helicopter surpassed the safe landing limits. This provides insight to the aircraft limitations that exist at a certain initial altitude and airspeed.

The Autorotation Index (AI) given in Equation 4.1 was implemented to determine if the index possesses any strong correlation with when the landing safety limits are exceeded. According to Leishman [27], a lower AI correlates to worse autorotation capabilities.

$$AI = \frac{I_R \Omega_0^2}{2WDL} \tag{4.1}$$

4.4.1 Effect of Gross Weight

One of the most significant factors affecting a helicopter's autorotation performance is its gross weight, which is why flight manuals have separate HV diagrams for different weights. Figure 4.16 shows the migration of the landing velocities as the AI varies as a result of changing the helicopter gross weight. The blue points represent the gross weight as it increases incrementally by 100 pounds. The red lines represent the boundary limitations for a safe landing.

As expected, an increase in gross weight decreases the helicopter's autorotation performance. By comparing Figures 4.16a-4.16c, it appears that the separation between a safe and unsafe landing is more sensitive to increases in gross weight at higher initial heights than at lower initial heights. Looking at the values for the AI supports

that inference. The first weight over the safety limit for the hover at 30 feet test case 16,900 lbs, which correlates to an AI of approximately 15.6. Meanwhile the first weight over the safety limit for the hover at 160 feet test case is 16,500 lbs, which correlates to a higher AI of 16.4.

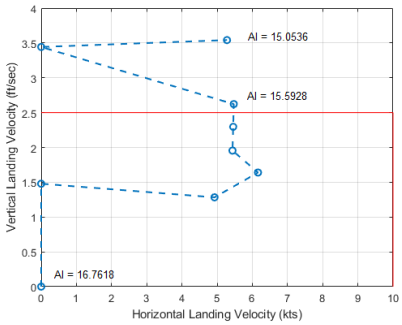

(a) Hover at 30 ft

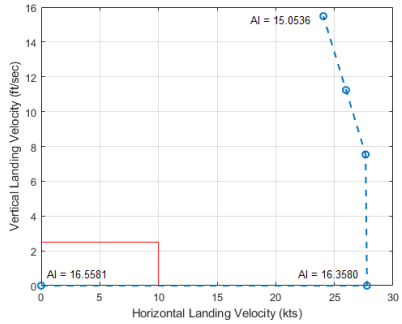

(b) Hover at 160 ft

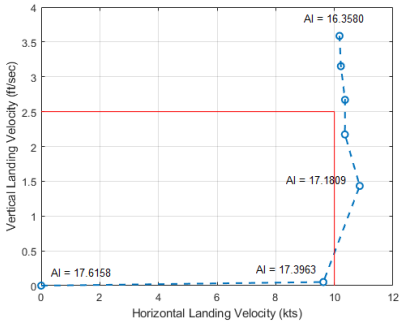

(c) Airspeed of 2 kts at 40 ft

Figure 4.16. Variation in Autorotation Index by Changing Gross Weight

4.4.2 Effect of Rotor Radius

Figure 4.17 shows the landing velocities as the main rotor radius changes in one foot increments. With a rotor radius of 25 feet, the helicopter is able to touchdown with zero velocity for each of these three test cases. As rotor radius is reduced, the landing velocity increases substantially. Similarly to changes in gross weight, changes to the rotor radius have a more pronounced effect on the landing velocities starting from a higher initial height. For the test cases shown in Figures 4.17a and 4.17b, the safe landing limits are surpassed at a rotor radius of 22 feet and 23 feet, and an AI of 14.3 and 17.0, respectively.

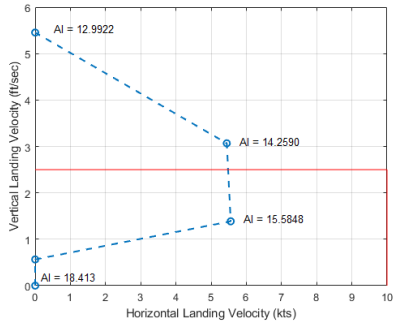

(a) Hover at 30 ft

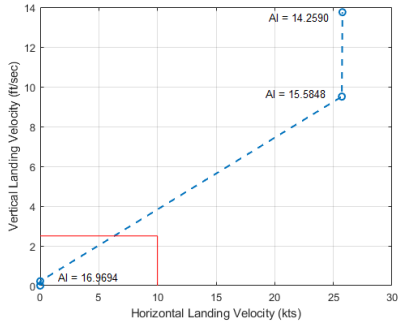

(b) Hover at 160 ft

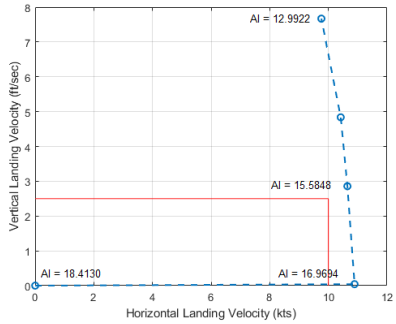

(c) Airspeed of 2 kts at 40 ft

Figure 4.17. Variation in Autorotation Index by Changing Rotor Radius

4.5 Chapter Summary

This chapter presented the solutions to the optimal control problem using GPOPS-II. The compilation of the optimal control solutions produced a grid of safe and unsafe landing conditions that outlined the HV curve. Along with a full HV diagram using the Hayden ground effect model, partial diagrams were presented for five other ground effect models as well as for variations of the Hayden ground effect factor. Lastly, the influence of changing the helicopter parameters of gross weight and rotor radius was presented.

V. Conclusions and Recommendations

5.1 Conclusions

Most of the main research objectives listed in Chapter 1 were achieved. A mathematical model for helicopter dynamics was developed and implemented into an optimal control problem. The model used for this research could be improved upon as discussed below in Section 5.2. The optimal control problem minimizing landing velocity was solved using pseudospectral collocation methods and nonlinear programming (NLP) via GPOPS and SNOPT to produce the helicopter's trajectory during autorotation. The solutions to several iterations of this problem at varying initial altitudes and airspeeds were compiled to produce a Height-Velocity (HV) diagram. Changes in the helicopter model parameters were then investigated. The main conclusions from this research are given below.

5.1.1 HV Diagram Construction

The iterative approach to solving for minimized landing velocities proved to be an effective methodology in constructing an HV diagram and delineating between safe and unsafe flight regions. This method allows for additional insight that other methods do not, since it solves the optimal landing velocity for initial conditions surrounding the HV curve in addition to points along the curve itself. Knowing the landing capabilities for more test cases allows for more confidence in the accuracy of the HV curve. Being able to solve for a wider variety of initial heights and airspeeds also reduces convergence issues when solving the optimal control problem.

5.1.2 Ground Effect

A proper ground effect model must be included in the helicopter dynamic model in order to obtain accurate solutions using the techniques utilized during this research. Excluding ground effect from the dynamic model or including a ground effect model whose ground effect factor is lower than 1.2 does not allow for an effective flare as the helicopter approaches the ground. Without the increased thrust provided by ground effect, the helicopter is unable sufficiently slow down before impact. Partial HV diagrams were constructed using five different models for ground effect factor. Based on the six models analyzed during this research, the models that did not incorporate blade element theory produced more conservative HV curves.

5.1.3 Autorotation Index

The Autorotation Index (AI) was implemented to provide a means of comparing autorotation capabilities between helicopters with different characteristics. The two helicopter parameters presented were helicopter gross weight and main rotor radius. As the gross weight increases, the AI decreases, and the helicopter lands with an increased velocity. Meanwhile, the AI increases as the rotor radius increases, resulting in the helicopter being able to land with a lower velocity. One noteworthy observation was that a higher AI is required to land safely from a higher initial height than is required to land safely from a lower initial height.

5.2 Recommendations for Future Work

The work accomplished during this research can be continued and improved upon in a number of ways. Below are some areas for future work and improvement.

5.2.1 Improvements to the Dynamic Model

One area of improvement would be to expand the dynamic model used in this research to include the derivatives of thrust and angle of attack. This would allow for limits to be placed on the rates of change for these variables, which would produce more realistic solutions. Solutions from models that include these derivatives as extra variables, such as the models used by Harris in [2], could then be compared to these solutions to estimate the effect that having rate limits on the control variables has on the HV diagram. In addition to adding the derivatives for thrust and rotor tip-path-plane angle of attack, a pilot model could be incorporated to provide optimal solutions that can actually be implemented during flight.

5.2.2 Collective Pitch

One of the initial goals of this research was to develop an additional dynamic model that contained collective pitch as a control variable instead of the current control variable of thrust. The reasoning behind including collective pitch as a control is that that would more accurately reflect the control inputs that a helicopter pilot actually uses while flying. Developing this type of dynamic model would require a further incorporation of blade element theory. Johnson [7] provides possible iterative methods for calculating induced velocity that could be used when replacing thrust with collective pitch in the dynamic model.

5.2.3 Autorotation Index Study

The study analyzing the effect of varying helicopter parameters could be continued to include the influence of factors such as rotor speed or solidity. Due to the nondimensional nature of the dynamic model, further studies should include nondimensional factors. Further analysis of the correlation between the AI and the capability for a

safe landing would also be beneficial. Different calculations for an autorotation index, such as those discussed in Section 2.7, could be compared.

5.3 Summary

This research produced an HV diagram using a 7-state helicopter model that was incorporated into an optimization problem to determine minimum landing velocities. The applied methodology reduced solution convergence issues that were present in prior research, and consequently provided a more robust way to determine the HV curve. Additional HV diagrams were created using alternative methods for calculating the ground effect factor. These diagrams showed the importance that ground effect plays during an autorotation landing and the necessity to include a proper ground effect model. The effect of variations of a few helicopter properties was also examined. This research provides a methodology for composing an HV curve analytically as well as examining factors that influence the HV curve.

Bibliography

[1] Y. Okuno *et al.*, "Analytical Prediction of Height-Velocity Diagram of a Helicopter Using Optimal Control Theory," *Journal of Guidance, Control, and Dynamics*, vol. 14, no. 2, pp. 453–459, 1991.

[2] M. J. Harris, "Analytical Determination of a Helicopter Height Velocity Diagram," M.S. Thesis, Air Force Institute of Technology, 2018.

[3] "ASYS 771 Lecture Notes," Department of Aeronautics and Astronautics, Air Force Institute of Technology, 2019.

[4] W. Johnson, "Helicopter Optimal Descent and Landing After Power Loss," NASA Ames Research Center, Tech. Rep. NASA-TM-73244, 1977.

[5] U. A. M. Command, "Engineering Design Handbook: Helicopter Engineering, Part One, Preliminary Design," Alexandria, VA, 1974.

[6] "Rotorcraft Flying Handbook," U.S. Department of Transportation, Federal Aviation Administration, 2000.

[7] W. Johnson, *Rotorcraft Aeromechanics*. New York, NY: Cambridge University Press, 2013.

[8] L. M. Free and L. J. Hepler, "Height-Velocity Test AH-1G Helicopter at Heavy Gross Weight," United States Army Aviation Systems Test Activity, Tech. Rep. 74-19, 1974.

[9] F. O'Hara and H. A. Mather, "The Performance after Power Failure of a Helicopter with Blade Pitch Control," Aeronautical Research Council, Tech. Rep. No. 2797, 1951.

[10] W. J. Hanley and G. Devore, "An Analysis of the Helicopter Height Velocity Diagram Including a Practical Method for its Determination," Aircraft Development Service, Federal Aviation Administration, Tech. Rep. NA-67-1, 1968.

[11] R. J. Pegg, "An Investigation of the Helicopter Height-Velocity Diagram Showing Effects of Density Altitude and Gross Weight," National Aeronautics and Space Administration, Tech. Rep. NASA TN D-4536, 1968.

[12] R. E. Studwell, "Helicopter Dynamic Performance Program Volume I - Engineer's Manual USARTL- TR-79-27A," Sikorsky Aircraft Division, United Technologies Corporation, Tech. Rep., 1980.

[13] D. E. Kirk, *Optimal Control Theory: An Introduction.* Englewood Cliffs, NJ: Prentice-Hall, Inc., 1970.

[14] J. T. Betts, *Practical Methods for Optimal Control and Estimation using Nonlinear Programming.* Seattle, WA: The Boeing Company., 2008.

[15] ——, "A Survey of Numerical Methods for Trajectory Optimization," *Boeing Information and Support Services*, 1998.

[16] A. V. Rao, "A Survey of Numerical Methods for Optimal Control," in *2009 AAS/AIAA Astrodynamics Specialist Conference, AAS Paper 09-334*, Pittsburgh, PA, 2009, pp. 533–541.

[17] J. S. Arora, *Introduction to Optimum Design*, 4th ed. Cambridge, MA: Academic Press, 2017.

[18] P. E. Gill *et al.*, "SNOPT: An SQP Algorithm for Large-Scale Constrained Optimization," *SIAM Journal on Optimization*, no. 4, 2002.

[19] M. A. Patterson and A. V. Rao, "GPOPS-II: A MATLAB Software for Solving Multiple-Phase Optimal Control Problems Using hp-Adaptive Gaussian Quadrature Collocation Methods and Sparse Nonlinear Programming," *ACM Transactions on Mathematical Software*, vol. 41, no. 1, 2014.

[20] D. Garg *et al.*, "Direct Trajectory Optimization and Costate Estimation of Finite-Horizon and Infinite-Horizon Optimal Control Problems Using a Radau Psudospectral Method," *Computational Optimization and Applications*, vol. 49, pp. 335–358, 2011.

[21] A. Y. Lee, "Optimal Landing of a Helicopter in Autorotation," Ph.D. dissertation, Stanford University, 1985.

[22] R. T. N. Chen and Y. Zhao, "Optimal Trajectories for the Helicopter in One-Engine-Inoperative Terminal-Area Operations," NASA Ames Research Center, Tech. Rep. 110400, 1996.

[23] E. B. Carlson and Y. J. Zhao, "Prediction of Tiltrotor Height-Velocity Diagrams Using Optimal Control Theory," *Journal of Aircraft*, vol. 40, no. 5, 2003.

[24] E. N. Bachelder *et al.*, "Improved Methods for Evaluating OEI Height-Velocity Boundaries," *American Helicopter Society Vertical Lift Aircraft Design Conference*, 2006.

[25] T. Wood, "High Energy Rotor System," in *American Helicopter Society 32nd Annual National V/STOL Forum*, Washington, D.C., 1976.

[26] E. Fradenburgh, "A Simple Autorotative Flare Index," *Journal of the American Helicopter Society*, vol. 29, pp. 73–74, 1984.

[27] J. G. Leishman, *Principles of Helicopter Aerodynamics*. Cambridge, MA: Cambridge University Press, 2002.

[28] B. L. Aponso *et al.*, "Evaluation of a Rotorcraft Autorotation Training Display on a Commercial Flight Training Device," *Journal of the American Helicopter Society*, vol. 52, no. 2, pp. 123–133, 2007.

REPORT DOCUMENTATION PAGE

Form Approved
OMB No. 0704–0188

1. REPORT DATE *(DD–MM–YYYY)*	2. REPORT TYPE	3. DATES COVERED *(From — To)*
14 September 2020	Master's Thesis	1 April 2019 — 14 September 2020

4. TITLE AND SUBTITLE

INVESTIGATION OF FACTORS IMPACTING A HELICOPTER HEIGHT-VELOCITY DIAGRAM

5a. CONTRACT NUMBER

5b. GRANT NUMBER

5c. PROGRAM ELEMENT NUMBER

6. AUTHOR(S)

Brown, Timothy, 1st Lt, USAF

5d. PROJECT NUMBER

5e. TASK NUMBER

5f. WORK UNIT NUMBER

7. PERFORMING ORGANIZATION NAME(S) AND ADDRESS(ES)

Air Force Institute of Technology
Graduate School of Engineering and Management (AFIT/EN)
2950 Hobson Way
WPAFB OH 45433-7765

8. PERFORMING ORGANIZATION REPORT NUMBER

AFIT-ENY-MS-20-S-084

9. SPONSORING / MONITORING AGENCY NAME(S) AND ADDRESS(ES)

AIR VEHICLE ENGINEERING DEPARTMENT 4.3
Attn: Steven Woods, Bldg. 2187
Naval Air Warfare Center Aircraft Division
48110 Shaw Road, Suite 1320
Patuxent River, MD 20670-1907

10. SPONSOR/MONITOR'S ACRONYM(S)

NAVAIR

11. SPONSOR/MONITOR'S REPORT NUMBER(S)

12. DISTRIBUTION / AVAILABILITY STATEMENT

DISTRIBUTION STATEMENT A:
APPROVED FOR PUBLIC RELEASE; DISTRIBUTION UNLIMITED.

13. SUPPLEMENTARY NOTES

14. ABSTRACT

A dynamic helicopter model was incorporated into an optimal control problem to determine minimal landing velocities. The solutions were determined using pseudospectral collocation methods as implemented by the GPOPS-II software. These solutions were then compiled to develop a HV diagram. An HV diagram displays regions of flight based on a helicopter's airspeed and height above the ground in which a safe landing would not be possible following engine failure. The applied methodology for constructing the HV diagram reduced issues involving solution convergence that was encountered in previous research. The influence of ground effect on the dynamic model was also investigated. After analyzing the HV diagrams constructed using five additional ground effect models, the significant impact that a chosen ground effect model has in the overall dynamic model was apparent. Finally, the effect that modifying certain helicopter parameters has on the helicopter's autorotation performance was considered. Optimal control solutions showed a decrease in autorotation capabilities for the case of an increased gross weight as well as for the case of a decreased rotor size.

15. SUBJECT TERMS

Height Velocity, Optimal Control, Autorotation

16. SECURITY CLASSIFICATION OF:			17. LIMITATION OF ABSTRACT	18. NUMBER OF PAGES	19a. NAME OF RESPONSIBLE PERSON
a. REPORT	b. ABSTRACT	c. THIS PAGE			Dr. Donald L. Kunz, AFIT/ENY
U	U	U	UU		19b. TELEPHONE NUMBER *(include area code)* (937) 255-3636 x4548; donald.kunz@afit.edu